Response of RC panels accounting for crack development and its interaction with rebars

Eckart Hars
Technical expert for maintenance planning, Swiss Federal Road Authority, Thoune, Switzerland (Orcid:0000-0001-8993-6937)

Filip Niketić
Research assistant and PhD candidate, École Polytechnique Fédérale de Lausanne, Lausanne, Switzerland (corresponding author: filip.niketic@epfl.ch) (Orcid:0000-0001-9106-1674)

Miguel Fernández Ruiz
Lecturer and senior scientist, École Polytechnique Fédérale de Lausanne, Lausanne, Switzerland (Orcid:0000-0001-6720-8162)

The response of reinforced concrete (RC) elements subjected to in-plane shear and axial stresses is governed by various potential failure mechanisms. For structural panels subjected to uniform stress states, their ultimate strength can be governed by yielding of the reinforcement, crushing of the concrete struts, sliding along a failure plane or spalling of the concrete cover. Although some expressions have been proposed in the literature to address this issue, they normally are empirical or semi-empirical in nature and do not distinguish among the failure mechanisms and their interaction. The purpose of this paper is to derive a mechanically-based efficiency factor for concrete in compression that is able to predict the actual behaviour of structural cracked concrete. This approach is shown to suitably predict the various potential failure modes and the development of the secondary shear cracks as well as the interaction between the reinforcement and the concrete.

Notation

b_w	thickness of analysed panel
c	concrete cover
D_{max}	maximum aggregate diameter
E_s	Young's modulus of elasticity of steel
F	applied force
f_c	concrete compressive strength
f_{cc}	confined concrete strength
f_{ce}	effective cylinder concrete compressive strength
f_{ctm}	tensile concrete strength
f_y	steel yield strength
h	size of panel in z-direction
l	size of panel in x-direction
$l_{cr,i}$	length of initial crack
l_{dow}	dowelling length
M	applied bending moment
M_{dow}	dowelling moment of plastic hinge
M_p	maximum bending moment carried by a rebar
N	normal force
N_{dow}	normal force in plastic hinge
N_p	maximum axial force carried by a rebar
R	reaction force
s_{rm}	average initial crack spacing
s_x, s_z	spacing between rebars in x- and z-directions
s_τ	relative amount of damaged struts
V_{dow}	dowelling shear force taken by a rebar
V_{xz}	applied shear force
w	crack width
w_{ini}	initial crack width
α	rebar tilting due to dowelling
δ	slip of plastic hinge
Δ	rebar elongation due to dowelling
ε_i	average strain in i-direction
ε_s	steel strain
η_{fc}	effectiveness factor for concrete brittleness
η_s	effectiveness factor considering the presence of reinforcement
η_ε	effectiveness factor considering induced transverse strains
η_τ	effectiveness factor considering the presence of initial cracks
θ	direction of principal compressive stress (and strain)
θ_{cr}	initial crack inclination
θ_{ult}	ultimate crack inclination
ρ	reinforcement ratio
σ	applied stress
σ_c	stress in concrete
σ_{cc}	effective confined concrete strength
$\sigma_{i,ult}$	applied stress in i-direction at failure
$\sigma_{i,y}$	applied stress in i-direction at the moment of first yielding
σ_s	stress in steel
$\sigma_{s,cr}$	stress in steel at the point of cracking
τ	applied shear stress
τ_b	reinforcement bond stress
τ_{cr}	shear stress transferred though a crack
τ_{ij}	applied shear stress
ϕ	rebar diameter

Introduction

One of the most significant challenges in the analysis of structural concrete elements is related to the fact that the resistance of a member depends on its state of strains and is thus

Magazine of Concrete Research

Response of RC panels accounting for
crack development and its interaction
with rebars
Hars, Niketić and Fernández Ruiz

gradually changing as the load level increases. In order to predict a realistic response, it is therefore crucial to investigate the dependency of the various load-carrying actions on the state of the strains as well as their interaction.

With respect to linear members (refer to Figure 1), it is clear that the state of stresses of the web and the two flanges are quite different. In the flanges, both materials (concrete and steel) are predominantly subjected to uniform tension or compression. The web, however, transfers shear, which requires simultaneous activation of the reinforcement in tension and concrete in compression. Activation of the reinforcement generates additional cracking and bond stresses associated with tangential tensile stresses (Tepfers, 1979). In addition, disturbance is created by the local dowelling of the bars and the discontinuities introduced by the presence of the bars (Muttoni *et al.*, 2006), reducing both the compressive strength and deformation capacity of concrete. Another important issue of the response of a panel is that, depending on the angle between the cracks and the direction of the principal compressive stress, the resistance of the material changes. The surface of the cracks is rough, which means that the average concrete compressive strength depends on the amount of stress that can be transferred by interface roughness. Given the fact that cracks are never perfectly parallel to each other and that they are actually unevenly spaced, local eccentricities appear inside the concrete struts, which can additionally reduce their strength.

Many experimental programmes have been conducted in attempts to better understand this complex problem (André, 1987; Belarbi and Hsu, 1995; Hsu and Zhang, 1997; Kirschner, 1986; Kollegger and Mehlhorn, 1990; Marti and Meyboom, 1992; Pang and Hsu, 1995; Schäfer *et al.*, 1990; Vecchio and Chan, 1990; Vecchio and Collins, 1982; Vecchio *et al.*, 1994; Watanabe and Muguruma, 1989; Zhang and Hsu, 1998), and the results from these studies are now incorporated in most modern codes of practice such as ACI 318-08 (ACI, 2008), Eurocode 2 (CEN, 2004) and the *fib* Model Code 2010 (*fib*, 2011), as well as in non-linear numerical methods. Usually, this phenomenon is accounted for by means of
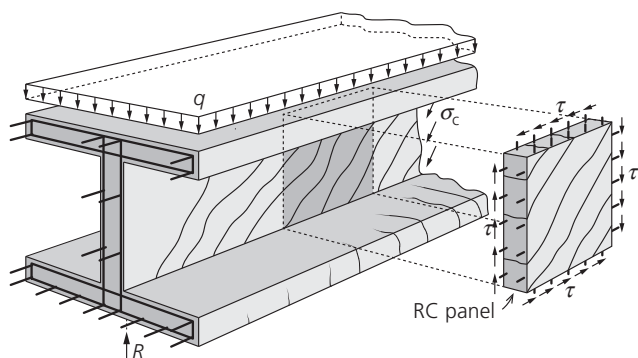
a strength reduction factor for concrete, which depends upon the cracking state and reduces the uniaxial strength of concrete.

In general, the two fundamental approaches used to address this problem are as follows.

- To fix the angle of the cracks in the element and limit the amount of compressive stress that can be transferred through such cracks. These are referred to as fixed crack models as proposed by, for example, Okamura and Maekawa (1991).
- To assume that the inclination of the crack is always parallel to the principal compressive stress direction (thus being free to rotate) while limiting the strength of concrete as a function of the acting tensile strains. These are known as rotating crack models.

One of the most commonly used expressions for limiting the concrete compressive strength in the rotating crack model approach is that proposed by Vecchio and Collins (1986) as part of the modified compression field theory (MCFT). This expression is

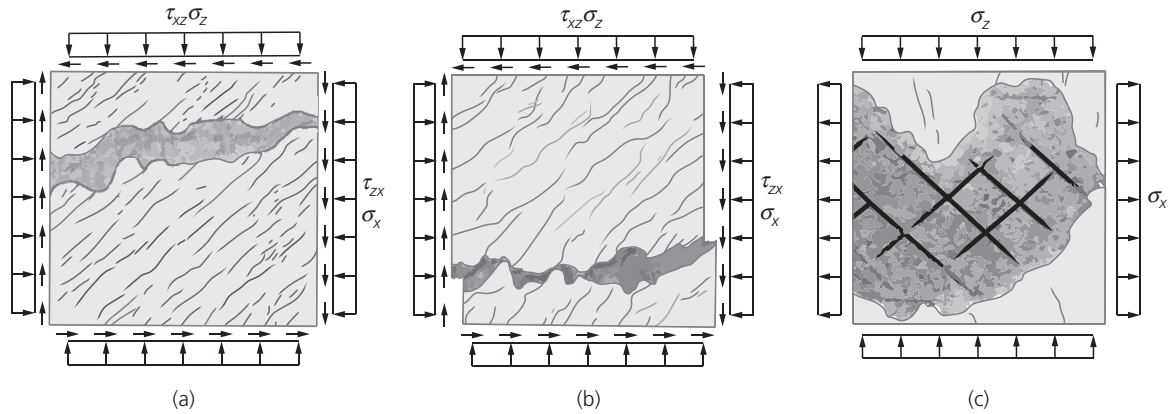1. $$\eta_\varepsilon = \frac{1}{0 \cdot 8 + 170\varepsilon_1}$$

where ε_1 is the average principal tensile strain of the structural panel.

This approach has been shown to be simple and robust for design and assessment, and can be easily implemented in a numerical manner (Fernández Ruiz and Muttoni, 2007; Muttoni *et al.*, 2015).

Other softening equations have been proposed by Belarbi and Hsu (1995), Kaufmann and Marti (1998) and Hars (2006). Vecchio (2000) derived another approach for dealing with shear failures of structural panels. Called the disturbed stress field model, the assumption of parallelism between the principal concrete stresses and strains is disregarded. Instead, the principal stresses turn after the principal concrete strains. The reduction of concrete compressive strength is still dependent on the average principal tensile strains.

Despite the fact that the compression softening equation of Vecchio and Collins (1986) suitably predicts experimental evidence, it is actually semi-empirical and does not distinguish between the various potential failure modes of (refer to Figure 2)

- crushing of the concrete strut
- sliding of the concrete
- spalling of the concrete cover.

Figure 1. RC beam and web panel subjected to shear

Magazine of Concrete Research

Response of RC panels accounting for crack development and its interaction with rebars
Hars, Niketić and Fernández Ruiz

Figure 2. Failure mechanisms of RC panels tested by Kollegger and Mehlhorn (1990): (a) crushing of panel PK07; (b) sliding of panel PK02; (c) concrete cover spalling of panel EGE6F4

This does not allow designers to suitably understand the mechanisms governing failure and their interaction, or how to enhance the behaviour in the most effective manner.

The purpose of this paper is to provide a mechanical approach to assess the concrete compressive strength efficiency factor by taking into account the actual behaviour of structural panels and the interactions between steel and concrete. The consistency of the approach is validated by means of extensive comparisons with available test data, and the formulation is used to understand the relationship and dependency among the various mechanical parameters implied.

Mechanical model for compression softening in reinforced concrete (RC) panels

The response of an RC panel subjected to shear and/or to biaxial tension/compression can be described by analysing three physical stages (Figure 3).

■ The first stage corresponds to a load transfer action valid up to first cracking of the panel (Figure 3(a)).
■ The second stage (Figure 3(b)) describes behaviour that is applicable between first cracking of the panel and yielding of the reinforcement in one direction (this phase is also valid in the case where a panel fails prior to yielding of any steel).
■ The third and final stage (Figure 3(c)) covers the loading history between yielding of the reinforcement in one direction and failure of the panel (due to crushing of the concrete or yielding of the reinforcement in both directions).

Stages of behaviour

The behaviour of a panel is characterised for an element as shown in Figure 4(a). The notations indicated in Figures 4(b)

and 4(c) are used to refer to the stress and strain states, respectively.

First stage: Linear elastic response

During the early phases of loading, a RC panel can be analysed assuming linear elastic behaviour. Once the tensile strength of concrete is reached, cracks start to develop (Figure 3(a)). As the direction of the principal tensile strains can be assumed to be parallel to the principal tensile stresses for the elastic response, the stress state, strain state and the initial cracking angle (θ_{cr}) are unambiguously defined (Figure 3(a)).

The amount of stress acting along the edge of a panel at any given point in the load history can be defined using the applied force as follows (refer to Figure 4(a)).

2. $\quad \sigma_x = \dfrac{F_x}{h b_w} = v_x$

3. $\quad \sigma_z = \dfrac{F_z}{l b_w} = v_z$

4. $\quad \tau_{xz} = \dfrac{V_{xz}}{lh} = v_{xz}$

F_x is the applied force in the x-direction, F_z is the applied force in the z-direction, V_{xz} is the applied shear force, l is the size of the panel in the x-direction, h is the size of the panel in the z-direction and b_w is the thickness of the panel.

Assuming that the panel behaves as a uniform elastic continuum up to cracking, one can calculate the principal tensile
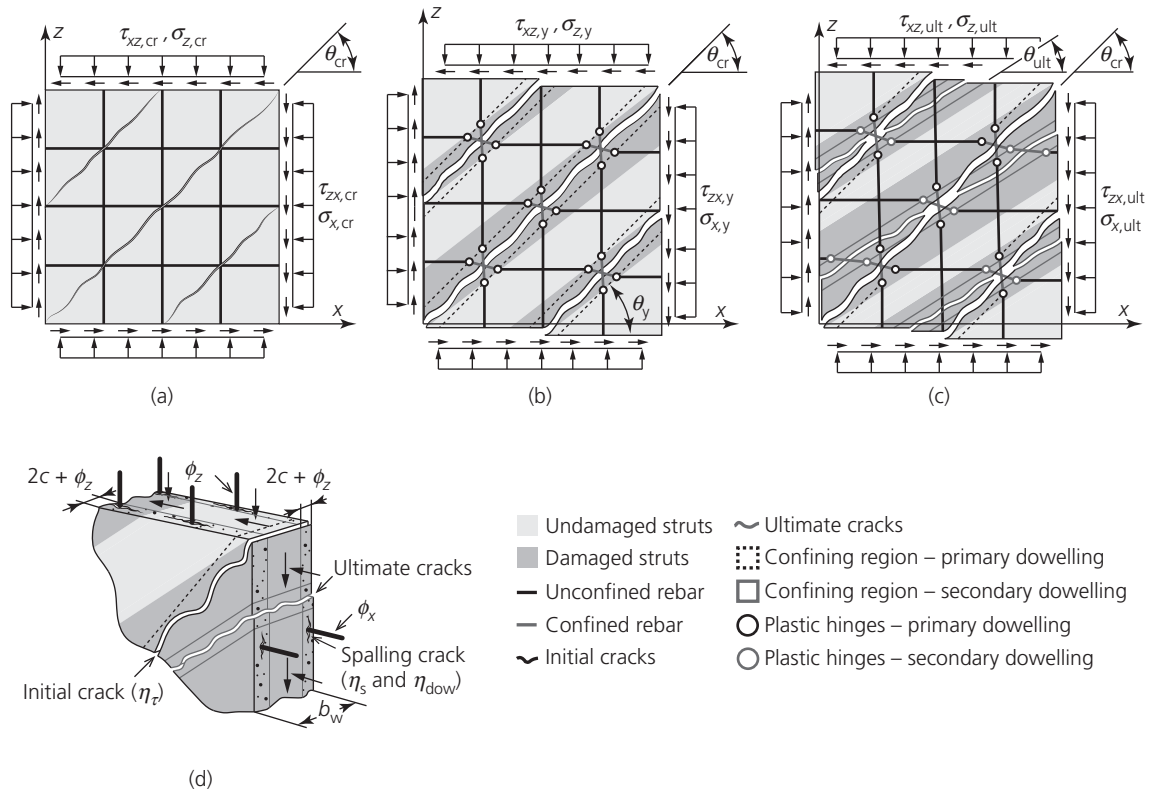
Magazine of Concrete Research

Response of RC panels accounting for
crack development and its interaction
with rebars
Hars, Niketić and Fernández Ruiz

Figure 3. Modelling the physical behaviour of a RC panel subjected to shear and axial loads: (a) cracking point; (b) onset of yielding; (c) failure of the panel; (d) in-plane and out-of-plane reduction mechanism of concrete compressive strength
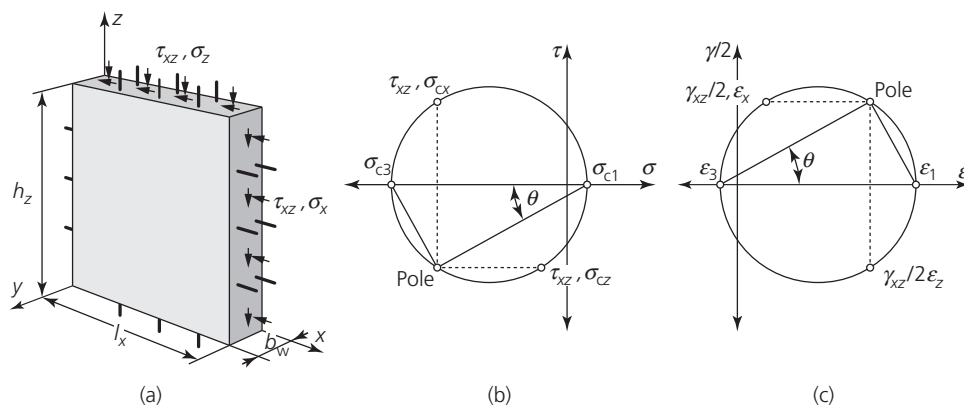

Figure 4. (a) Geometry and loading properties of an analysed panel. (b) Stress state of a concrete strut. (c) Average strain state of the panel

stress of the panel as

5.
$$\sigma_{c1} = \frac{v_x + v_z}{2} + \sqrt{\left(\frac{v_x - v_z}{2}\right)^2 + v_{xz}^2}$$

The limit case of the elastic phase is reached when the principal tensile stress becomes equal to the mean tensile strength of concrete ($\sigma_{c1} = f_{ctm}$). According to *fib* Model Code 2010

(*fib*, 2011), this can be estimated as

6.
$$f_{ctm} = \begin{cases} 0 \cdot 3(f_c)^{2/3} & \text{for } f_c \leq 50 \text{ MPa} \\ 2 \cdot 12 \ln(1 + 0 \cdot 1 f_c) & \text{for } f_c > 50 \text{ MPa} \end{cases}$$

where f_c is the uniaxial concrete compressive strength measured in a cylinder.

4

Magazine of Concrete Research

Response of RC panels accounting for crack development and its interaction with rebars
Hars, Niketić and Fernández Ruiz

The initial cracking angle can now be determined using Mohr's transformations (Figure 4(b)) as follows

7. $\qquad \tan \theta_{cr} = \dfrac{\sigma_{cx} - \sigma_{c3}}{\tau_{xz}}$

Second stage: Cracked behaviour

The initial cracking angle remains unchanged throughout the second stage (as presented in Figure 3(b)). However, the direction of the principal compressive stresses starts to rotate in order to remain parallel to the principal compressive strains (θ_y in Figure 3(b)). This means that a portion of the concrete compressive struts, hereafter called the damaged struts, crosses the initial cracks (refer to Figure 3(b)). The strength of such struts is governed by aggregate interlocking occurring along the initial cracks. The remaining struts are considered as undamaged struts. Even though they are characterised by the absence of in-plane cracks, their strength is not equal to the concrete compressive strength determined from the standard cylinder test. This is justified, as the presence of the reinforcement induces the formation of spalling cracks, leading to out-of-plane failures (refer to Figure 3(d)). These spalling cracks limit the compressive strength of the concrete over a given portion of the panel's thickness (shown as the dotted areas in Figure 3(d)). This effect was taken into account based on the work of Hars (2006). The spalling reduction applies not only to the undamaged struts, but also to the damaged struts. In this manner, the strength of each strut is governed by the presence of in-plane and/or out-of-plane cracks.

The yield strength of the reinforcement is limited by the dowelling of the bars in the region near the cracks. As plastic hinges start to develop (indicated by the white circles in Figure 3(b)), the concrete between the surfaces of the cracks and the plastic hinges locally equilibrates the dowelling forces (shown as the light grey zones along the reinforcement in Figure 3(b)). This region, shown using dashed lines in Figure 3(b), which is partly developing in the undamaged and damaged struts, introduces a reduction in

concrete strength due to the out-of-plane tensile stresses, potentially leading to spalling failures (presented in Figure 2(c)).

Third stage: Behaviour after yielding

The third and final stage is presented in Figure 3(c). At this point, a second family of cracks develops. Their inclination is parallel to the direction of the principal concrete compressive stress (and strain) at failure (θ_{ult}). The presence of a second family of cracks causes additional dowelling of the reinforcement (plastic hinges activated at this phase are presented in Figure 3(c) using light grey circles). Given the fact that the direction of the principal compressive stress continues to rotate compared to the previous stage, the percentage of the surface corresponding to damaged struts increases and that of the undamaged struts decreases. The strength reduction mechanisms governing the strength of each type of concrete strut are methodologically the same as the previous stage. The stress field continues to rotate until the reinforcement in the other direction eventually reaches yielding or until the principal compressive stresses become equal to the effective concrete compressive strength.

Plastic strength of the reinforcement accounting for dowelling forces and bar elongation

As the initial and ultimate cracks start to open, the horizontal and vertical reinforcement of the panel is subjected to local bending. Consequently, plastic hinges start to develop in the vicinity of the crack faces (see Figures 3(b) and 3(c)), originating dowelling action. As the bar is dowelled, this reduces its capacity to carry tensile forces and determines the location at which plastic hinges will originate. Physical evidence of the dowelling action in RC panels has been reported by, for instance, Vecchio *et al.* (1994) in their experimental campaign. In addition to this, panels that have experienced sliding failures at the ultimate limit state (see Figure 2(b)) also show significant dowelling of the reinforcement.

The plastic stress distribution within a hinge at the ultimate limit state is presented in Figure 5(a). The central part of the
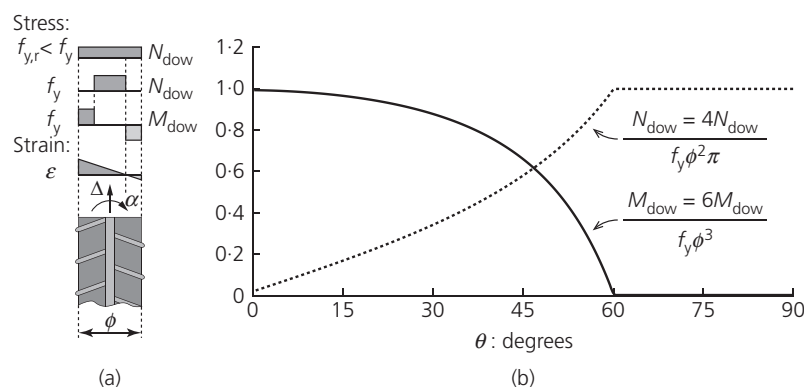

Figure 5. (a) Distribution of strains, stresses and internal force inside a plastic hinge of a rebar. (b) Axial strength reduction of horizontal rebar as a function of crack opening angle

Magazine of Concrete Research

Response of RC panels accounting for crack development and its interaction with rebars
Hars, Niketić and Fernández Ruiz

cross-section carries tension, while the rest carries the bending moment. In order to account for such interaction, the apparent yield strength of the steel in tension needs to be reduced ($f_{y,r}$). It must be noted, however, that this detrimental effect of the dowelling in one direction ($f_{y,r}$) brings some beneficial effects to the opposite direction (V_{dow}), as presented in Figures 6(d) and 6(e). This is justified as the bent rebar can resist some shear forces, reducing the amount of the force that has to be carried by the bars in the perpendicular direction. Depending on the inclination of the crack, the number of rebars that are actively contributing to carrying applied loads through the dowelling action can vary. When this angle is greater than 45° (see Figure 6(d)), the number of rebars is governed by their spacing (s_x and s_z) and the height of the panel (h), whereas if the angle is less than 45° (Figure 6(e)) the number of rebars is determined based on the length of the panel (l) and the spacing between rebars (s_x and s_z).

The development of tensile and dowel forces in a plastic hinge for a given crack direction and kinematics is investigated in Figure 6. The inclination of the initial crack is defined by θ_{cr} and the direction of its opening by θ. These two angles are considered to account for the fact that the crack is not necessarily (in all cases) parallel to the principal compressive stress and strain direction, and is therefore subjected to simultaneous opening and sliding. The plastic hinges are located at a distance to the crack called the dowelling length (l_{dow}) (see Figure 6(a)). When the crack opens, the plastic hinges move horizontally and vertically from each other (refer to

Figure 6(b)). Since the rebar is not perfectly bonded to concrete, it slips for a value that can be expressed as function of the corresponding crack width. This is defined by the coefficient ξ in Figure 6(c). Consequently, the rebar tilts (at a specific angle α) and elongates for 2Δ. Along the dowelling length, the rebar pushes against the surrounding concrete, transferring the dowelling forces to the concrete (σ_{cc}). According to Rasmussen (1962), the dowelling length for the case of dowelling with no eccentricity and no normal load can be estimated as

$$8. \qquad l_{dow} = \phi \sqrt{\frac{f_y}{3 f_{cc}}}$$

where l_{dow} is the dowelling length, ϕ is the diameter of the rebar, f_y is the initial yield strength of the rebar and f_{cc} is the concrete strength in a confining state.

Sorensen *et al*. (2016) state that, in the case of increased eccentricity and additional normal load, the dowelling length actually decreases, which reduces the moment contribution as well as the percentage of confining (i.e. damaged) struts within a panel (refer to Figures 3(b) and 3(c)). Therefore, the approach presented is slightly conservative.

The enhanced concrete strength equilibrating the dowelling forces can be estimated accounting for the influence of the concrete cover. Based on the work of Vintzeleou and Tassios
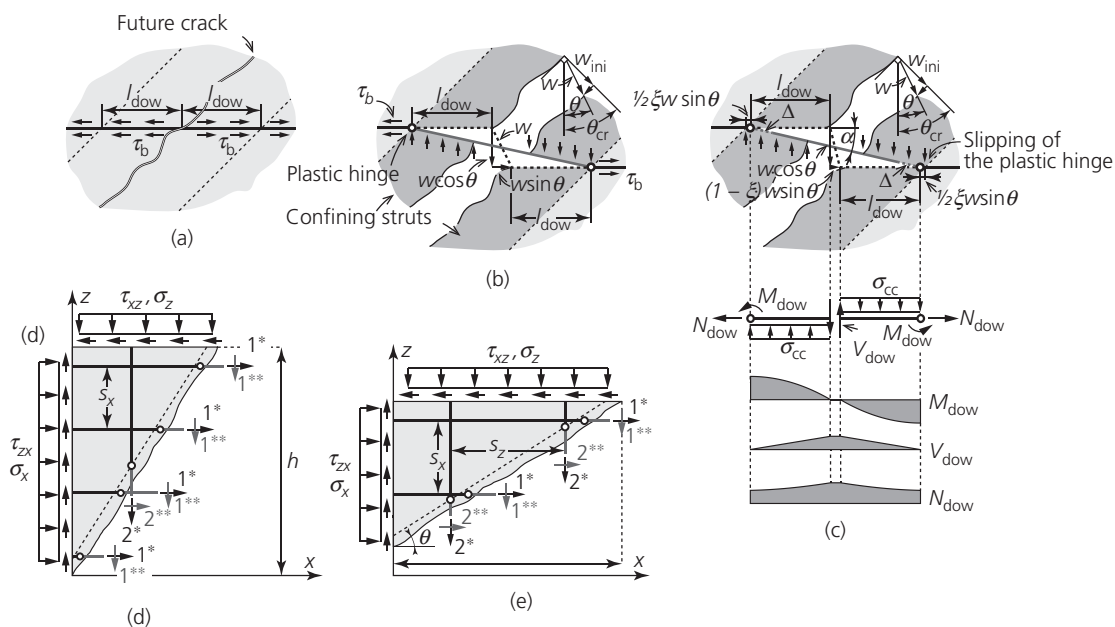
Figure 6. Dowelling mechanism of the reinforcement. (a) Location of the future plastic hinges and the initial crack. (b) Local bending of a horizontal rebar in the proximity of an initial crack – no slip along the rebar. (c) Local bending of a horizontal rebar in the proximity of an initial crack – accounting for the slip along the rebar. (d) Contributing rebars for crack angles greater than 45°. (e) Contributing rebars for crack angles less than 45°. 1*, $n_x f_{yx}$; 1**, $V_{x,dow}$; 2*, $n_z f_{yz}$; 2**, $V_{z,dow}$

Magazine of Concrete Research

Response of RC panels accounting for crack development and its interaction with rebars
Hars, Niketić and Fernández Ruiz

(1990), the confined concrete strength can be estimated as

9. $$f_{cc} = f_c \left[1 + \frac{c_1}{\phi} \left(0.02 \frac{c_2}{\phi} + 0.15 \right) \right]^2 \leq 5 f_c$$

where c_1 is the concrete cover perpendicular to the confining concrete stress (cannot be larger than 4ϕ) and c_2 is the concrete cover parallel to the confining concrete stress (cannot be larger than 8ϕ).

On average, the corresponding values for the confined concrete strength are approximately equal to $3.7 f_c$. The actual concrete strength (σ_{cc}) is, however, determined at a later stage accounting for the actual dowelling moment in the rebar (M_{dow}), and is always lower than f_{cc}.

Relative rebar slip is estimated using an effective tie, as shown in Figures 7(b) and 7(c). Starting from the geometry of an analysed panel (Figure 7(a)), the crack spacing is estimated using the expression assuming a constant bond strength according to Marti *et al.* (1998)

10. $$s_{rm} = \frac{1}{(\sin\theta_{cr}/s_{rmx}) + (\cos\theta_{cr}/s_{rmz})}$$

11. $$s_{rmx} = \frac{3}{2} \left(\frac{1 - \rho_x}{\rho_x} \right) \frac{\phi_x}{8}$$

12. $$s_{rmz} = \frac{3}{2} \left(\frac{1 - \rho_z}{\rho_z} \right) \frac{\phi_z}{8}$$

where ρ_x is the reinforcement ratio in the *x*-direction, ϕ_x is the diameter of the rebar in the *x*-direction, ρ_z is the reinforcement ratio in the *z*-direction and ϕ_z is the diameter of the rebar in the *z*-direction.

The effective reinforcement ratio in the direction perpendicular to the direction of cracks (Figure 7(b)) is calculated from

13. $$\rho_{eff} = \rho_x \sin^2\theta_{cr} + \rho_z \cos^2\theta_{cr}$$

The effective rebar spacing is assumed to be equal to the average spacing of the horizontal and vertical reinforcement projected in the direction of the cracks, given by

14. $$s_{eff} = \frac{1}{2} \left(\frac{s_x}{\sin\theta_{cr}} + \frac{s_z}{\cos\theta_{cr}} \right)$$

where s_x is the spacing between rebars in the *x*-direction and s_z is the spacing between the rebars in the *z*-direction.

Figure 7(c) shows the reinforcement strain distribution inside the effective tie at its cracking point and for a higher stress level. As can be seen in the figure, both strains are linearly varying between the two consecutive cracks (constant bond strength). Maximum steel strains (ε_{s1}) are expected at the location of the crack while minimum steel strains (ε_{s2}) are expected in the middle of the two consecutive cracks (concrete strains are neglected). These strains are given by

15. $$\varepsilon_{s1} = \frac{\sigma_s}{E_s}$$

16. $$\varepsilon_{s2} = \frac{\sigma_s}{E_s} - \frac{2\tau_b s_{rm}}{E_s \phi_{eff}}$$

where σ_s is the stress in the reinforcement, E_s is the Young's modulus of elasticity, ϕ_{eff} is the effective rebar diameter (shown in Figure 7(b)) and τ_b is the average bond stress, which can be estimated according to Marti *et al.* (1998) (for deformed rebars) from
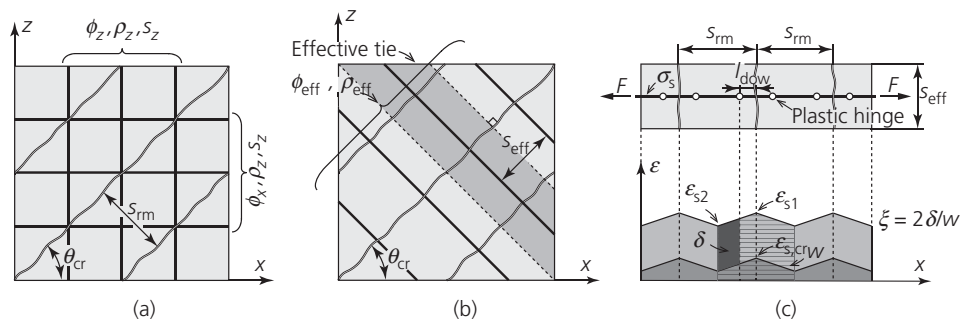
17. $$\tau_b = 2 f_{ctm}$$

Figure 7. (a) Geometry of the reinforcement in horizontal and vertical directions. (b) Geometry of the effective reinforcement and effective tie. (c) Strain state along the effective tie

Magazine of Concrete Research

Response of RC panels accounting for crack development and its interaction with rebars
Hars, Niketić and Fernández Ruiz

where f_{ctm} is the mean tensile concrete strength given in Equation 6.

In the case of smooth rebars, the bond law is calculated according to *fib* Model Code 2010 (*fib*, 2011) as

18. $\quad \tau_b = 0.15\sqrt{f_c}$

Plastic hinges are assumed to form at the cracking point of the panel in the vicinity of the initial cracks (as presented in Figure 7(c)). As the stress level increases in the rebar, the plastic hinges move towards the crack. The slip (δ) can be estimated by integrating the area hatched with lines in Figure 7(c). As presented in Figure 7(c), this value depends on the amount of steel stress (σ_s). A mean value between the steel stress at the point of cracking ($\sigma_{s,cr}$) and the yield strength of the steel (f_y) is assumed, in other words

19. $\quad \sigma_s = \dfrac{\sigma_{s,cr} + f_y}{2}$

20. $\quad \sigma_{s,cr} = \dfrac{f_{ctm}}{\rho_{eff}}$

The amount of slip itself can be estimated as

21. $\quad \delta = \dfrac{\sigma_s - \sigma_{s,cr}}{E_s}\left(\dfrac{s_{rm}}{2} - l_{dow}\right)$

In order to express the slip of a hinge in a more general manner (as a function of the corresponding crack width), the parameter ξ is defined as

22. $\quad \xi = \dfrac{2\delta}{w}$

23. $\quad w = s_{rm}\dfrac{\varepsilon_{s1} + \varepsilon_{s2}}{2}$

Based on the mechanism given in Figure 6(a), the rebar tilting angle can be expressed as

24. $\quad \alpha = \arctan\left(\dfrac{w\cos\theta}{2l_{dow} + (1-\xi)w\sin\theta}\right)$

Returning to the same mechanism, the rebar elongation can be determined from

25. $\quad (2l_{dow} + 2\Delta)^2 = [2l_{dow} + (1-\xi)w\sin\theta]^2 + (w\cos\theta)^2$

26. $\quad \Delta = \dfrac{1}{2}\sqrt{4l_{dow}^2 + 4l_{dow}w\sin\theta(1-\xi) + w^2[1 - 2\xi(\sin\theta)^2 + (\xi\sin\theta)^2]} - l_{dow}$

where w is the total displacement, which can be estimated according to the mechanism presented in Figure 6(b) as

27. $\quad w = \dfrac{w_{ini}}{\cos(\theta_{cr} - \theta)}$

where w_{ini} is the initial crack width.

In order to estimate the amount of rebar dowelling based on crack kinematics, it is necessary to define the incremental difference of the rebar tilting angle and its elongation as a function of the crack opening. In other words, one needs to find the first derivatives of Equation 24 and 26

28. $\quad \dot\alpha = \dfrac{\partial\alpha}{\partial w} = \dfrac{2l_{dow}\cos\theta}{4l_{dow}^2 + 4l_{dow}w\sin\theta(1-\xi) + w^2[1 - 2\xi(\sin\theta)^2 + (\xi\sin\theta)^2]}$

29. $\quad \dot\Delta = \dfrac{\partial\Delta}{\partial w} = \dfrac{2l_{dow}\sin\theta(1-\xi) + w[1 - 2\xi(\sin\theta)^2 + (\xi\sin\theta)^2]}{2\sqrt{4l_{dow}^2 + 4l_{dow}w\sin\theta(1-\xi) + w^2[1 - 2\xi(\sin\theta)^2 + (\xi\sin\theta)^2]}}$

The yield condition of the circular cross-section subjected to simultaneous tension and bending is similar to the one derived for a rectangular cross-section but far more complex (Sorensen *et al.*, 2016), which is why the dowelling of the rebar is derived using the simpler expression (Nielsen and Hoang, 2011)

30. $\quad f(N, M) = m + n^2 - 1 = 0$

31. $\quad m = \dfrac{M}{M_p} = \dfrac{6M}{\phi^3 f_y}$

32. $\quad n = \dfrac{N}{N_p} = \dfrac{4N}{\phi^2\pi f_y}$

Magazine of Concrete Research

Response of RC panels accounting for crack development and its interaction with rebars
Hars, Niketić and Fernández Ruiz

where M is the bending moment acting on a rectangular cross-section and N is the axial force acting on the rectangular cross-section.

Application of the normality condition of Equation 30 gives

$$33. \qquad \dot{\alpha} = \lambda \frac{\partial f(M,N)}{\partial M} = \lambda \frac{\partial f(M,N)}{\partial m} \frac{\partial m}{\partial M} = \lambda \frac{1}{M_\mathrm{p}}$$

$$34. \qquad \dot{\Delta} = \lambda \frac{\partial f(M,N)}{\partial N} = \lambda \frac{\partial f(M,N)}{\partial n} \frac{\partial n}{\partial N} = \lambda 2n \frac{1}{N_\mathrm{p}}$$

where λ is an integration factor.

After combining the Equations 28, 29, 33 and 34, it is possible to estimate the relative amount of axial tensile force in a rebar for given crack kinematics

$$35. \qquad n_\mathrm{dow} = \left[\frac{3\pi}{4\phi} \frac{2l_\mathrm{dow}\sin\theta(1-\xi) + w[1 - 2\xi(\sin\theta)^2 + (\xi\sin\theta)^2]}{4l_\mathrm{dow}\cos\theta} \right] \sqrt{4l_\mathrm{dow}^2 + 4l_\mathrm{dow}w\sin\theta(1-\xi) + w^2[1 - 2\xi(\sin\theta)^2 + (\xi\sin\theta)^2]}$$

Once the amount of axial tensile force in a rebar is determined, the amount of moment can be expressed as

$$36. \qquad m_\mathrm{dow} = 1 - n_\mathrm{dow}^2$$

The distribution of these two parameters (n_dow and m_dow) can be seen in Figure 5(b) as a function of the crack opening angle. As can be seen, the maximum amount of moment is obtained for $\theta = 0°$. At this angle, the crack opens perpendicularly to the rebar. For a general case (see point A in Figures 8(a) and 8(b)), the neutral axis is inside the analysed rebar, which means that part of the cross-section is subjected to uniform compression while the rest is subjected to uniform tension. When the bar is subjected to a pure normal force, the stress state of point B can be achieved through various strain profiles (see Figure 8(b)) since the neutral axis is always outside of the rebar cross-section. According to the rigid plastic approach, at point B, it is therefore possible to have no moment but some level of curvature.

The maximum shear carried by dowelling can be calculated accounting for the pressure developed in the concrete (Figure 6(c))

$$37. \qquad V_\mathrm{dow} = \phi l_\mathrm{dow}\sigma_\mathrm{cc}$$

where σ_cc is the effective concrete pressure acting along the dowel length, which may be estimated from simple free-body equilibrium (Figure 6(c))

$$38. \qquad \sigma_\mathrm{cc} = \frac{2M_\mathrm{dow}}{\phi l_\mathrm{dow}^2} = \frac{m_\mathrm{dow}\phi^2 f_\mathrm{y}}{3l_\mathrm{dow}^2}$$

The total force carried by the dowelling can thus be calculated on the basis of Figures 6(d) and 6(e) by adding the contribution of each bar (V_dow) for the total number of bars intersected by cracks.

Concrete strength limitations

The effective concrete compressive strength of the analysed panel can be expressed by combining the resistances of the two types of struts (damaged and undamaged) presented in Figure 9(a) in the following manner.

$$39. \qquad f_\mathrm{ce} = f_\mathrm{c}\eta_\mathrm{fc}[\eta_\mathrm{DS}s_\tau + \eta_\mathrm{UDS}(1 - s_\tau)]$$
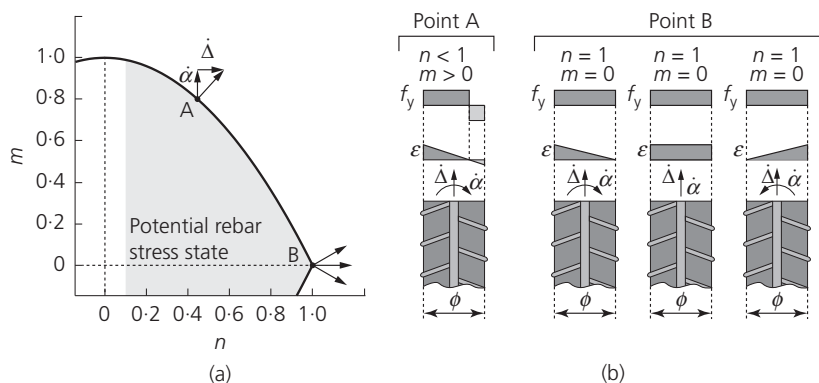
Figure 8. (a) Moment–normal force interaction diagram. (b) Distribution of strains and stresses in a rebar

Magazine of Concrete Research

Response of RC panels accounting for
crack development and its interaction
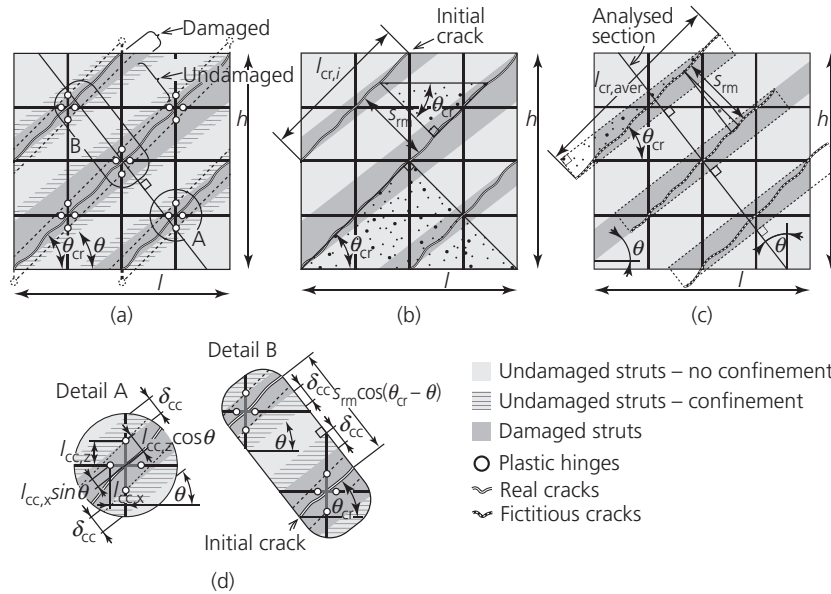with rebars
Hars, Niketić and Fernández Ruiz

Figure 9. (a) Surface quantity and distribution of damaged and undamaged struts in a panel. (b) Number of initial cracks in a panel. (c) Effective damaged strut length and width. (d) Details determining the confining concrete strut width

f_c is the uniaxial concrete compressive strength measured in a cylinder, s_τ is the relative amount of damaged struts in the panel, η_{DS} is the effectiveness factor for the compressive strength of damaged struts and η_{UDS} is the effectiveness factor for the compressive strength of undamaged struts.

The parameter η_{fc} is an effectiveness factor that accounts for the brittle behaviour of concrete in compression. The original expression for η_{fc} was proposed by Muttoni (1989) and is currently incorporated in *fib* Model Code 2010 (*fib*, 2011) for calculation of the compressive strength of concrete in shear

40. $\quad \eta_{fc} = \sqrt[3]{\left(\dfrac{30}{f_c}\right)} \leq 1{\cdot}0$

This factor allows one to account for the internal redistributions of stress occurring in the panel.

The relative amount of damaged (and consequently undamaged) struts in the analysed panel depends on the length of the initial cracks (which can be seen in Figures 9(a) and 9(b)). In order to account for their uneven length, an effective (average) crack length is calculated based on geometrical considerations from Figure 9(b)

41. $\quad l_{eff} = \left(\dfrac{l - 0s_{rmx}}{\cos\theta_{cr}} + 2\dfrac{l - 1s_{rmx}}{\cos\theta_{cr}} + 2\dfrac{l - 2s_{rmx}}{\cos\theta_{cr}} + \cdots + 2\dfrac{l - ns_{rmx}}{\cos\theta_{cr}}\right)/2n + 1 \; l_{eff} = \dfrac{l}{\cos\theta_{cr}} - \dfrac{s_{rm}}{\sin\theta_{cr}\cos\theta_{cr}}\left(\dfrac{n(n+1)}{2n+1}\right)$

where n can be calculated as

42. $\quad n = \dfrac{l\sin\theta_{cr}}{s_{rm}}$

Combining Equations 41 and 42 yields

43. $\quad l_{eff} = \dfrac{l}{\cos\theta_{cr}}\left(\dfrac{n}{2n+1}\right)$

Finally, the relative amount of damaged struts in the analysed section can be estimated (indicated in Figure 9(c)) by

44. $\quad s_\tau = \dfrac{n'l_{eff}\sin(\theta_{cr} - \theta)\cos\theta}{h}$

45. $\quad n' = \dfrac{h\cos(\theta_{cr} - \theta)}{\cos\theta s_{rm}} + 1$

where n' is the effective number of damaged struts, s_{rm} is the average initial crack spacing, l is the size of the analysed panel in the x-direction and h is the size of the analysed panel in the z-direction.

Strength of the damaged struts
The compressive strength of the damaged struts is limited by the parameter η_{DS}, which takes into account

■   the presence of the rebars in the concrete struts, governing the out-of-plane failures (η_s, in analogy with Hars (2006))

Magazine of Concrete Research

Response of RC panels accounting for crack development and its interaction with rebars
Hars, Niketić and Fernández Ruiz

- the presence of the initial cracks crossing the damaged struts, governing the in-plane element failures (η_τ, which will be defined later in the paper)
- the interaction between the in-plane and out-of-plane element failures (adopted from Hars (2006))
- the presence of dowelled rebars (η_{dow}, which will be defined later in the paper).

The value of the effectiveness factor for the compressive strength of the damaged struts can thus be calculated as

46.
$$\eta_{DS} = \min \begin{cases} \eta_s \\ \dfrac{\eta_\tau \max\left\{ \begin{array}{c} 0 \\ b_w - (4c + 2\phi_{ext}) \end{array} \right\}}{b_w} \\ + \dfrac{\eta_\tau \min\left\{ \begin{array}{c} b_w \\ 4c + 2\phi_{ext} \end{array} \right\}}{b_w}(1 - \eta_{dow}\delta_s) \end{cases}$$

where η_s is an effectiveness factor that accounts for the presence of the reinforcement in concrete (out-of-plane failure), η_τ is an effectiveness factor that accounts for the presence of the initial cracks in concrete (in-plane-failure), η_{dow} is a factor that takes into account the presence of rebars pressing against the concrete due to the dowelling (see Figure 3(c) and (d)), δ_s is the ratio between the external rebar diameter and the sum of twice the concrete cover thickness and the external rebar diameter, b_w is the thickness of the panel, and c is the concrete cover thickness.

With respect to Equation 46, it can be seen that the resistance of a damaged strut is limited either by the presence of out-of-plane cracks (considered by means of the coefficient η_s) or by the presence of in-plane cracks (considered by means of the coefficient η_τ) combined with the dowelling of the reinforcement (η_{dow}).

The effectiveness factor that accounts for the presence of reinforcement in concrete (η_s) was developed on the basis of the work of Hars (2006). Reinforcement bars introduce local defects into the concrete cover region, which may cause it to spall off (see the dotted strips in Figure 3(d)), while the rest of the section remains undisturbed. This effect is physically governed by the out-of-plane cracks (called spalling cracks in Figure 3(d)) and can be quite pronounced in the case of heavily reinforced concrete panels. On the basis of the work of Hars (2006), it is proposed that the effectiveness factor that accounts for the presence of the reinforcement in concrete (η_s) is evaluated as

Figure 10. (a) Stress state of a damaged strut and inclination of an initial crack. (b) Stresses acting along the sides of the analysed free body. (c) Shear stresses acting along the crack surface as a function of the stress field rotation angle

49.
$$\delta_s = \frac{\phi_{ext}}{2c + \phi_{ext}}$$

50.
$$\phi_s = \begin{cases} \arctan 0.6 & \text{for plain reinforcement bars} \\ \arctan 1.0 & \text{for ribbed reinforcement bars} \end{cases}$$

Here, c is the concrete cover, s_{ext} is the distance between external reinforcement bars, ϕ_{ext} is the external rebar diameter and ω_s is the local stress field disturbance ratio.

It should be noted that Equation 48 gives the expression for ω_s assuming that the external reinforcement is in the vertical direction. In the case where a horizontal rebar is closer to the panel's surface, $\cos\theta$ should be replaced by $\sin\theta$ in Equation 48.

As already mentioned, the effectiveness factor that accounts for the presence of the initial cracks in concrete (η_τ) limits the strength of the damaged concrete struts. This coefficient is estimated based on the amount of shear stress that can be transferred through the initial crack. By investigating a free body (Figures 10(a) and 10(b)), the equilibrium of forces acting along each side of the free body in the direction of the initial crack (θ_{cr}) can be obtained as

47.
$$\eta_s = \frac{\max\left\{ \begin{array}{c} 0 \\ b_w - (4c + 2\phi_{ext}) \end{array} \right\}}{b_w} + \frac{\min\left\{ \begin{array}{c} b_w \\ 4c + 2\phi_{ext} \end{array} \right\}}{b_w} \left\{ \frac{f_c^2}{225}\left[1 + \frac{4\omega_s^2}{\delta_s(1-\sin\phi_s)}\left(\frac{1-\delta_s(1-\sin\phi_s)}{1-\delta_s} \right)^2 \right]^{-1} + \frac{1}{1-\delta_s(1-\sin\phi_s)} \right\}^{-1}$$

48.
$$\omega_s = \min\left\{ \frac{s_{ext} - \phi_{ext}^{1.5}}{2\cos\theta} \frac{1}{2c + \phi_{ext}} \right\}$$

51.
$$\sigma_{c3}\sin(\theta_{cr}-\theta)\cos(\theta_{cr}-\theta) + \sigma_{c1}\cos(\theta_{cr}-\theta)\sin(\theta_{cr}-\theta) = \tau_{cr}$$

Magazine of Concrete Research

Response of RC panels accounting for crack development and its interaction with rebars
Hars, Niketić and Fernández Ruiz

Expressing the principal concrete compressive strength from Equation 51

52.
$$\sigma_{c3} = \frac{2\tau_{cr}}{\sin(2(\theta_{cr} - \theta))} - \sigma_{c1}$$

Since the concrete strength in this free body is limited by the amount of shear stress that can be transferred through a crack and the brittleness of the concrete

53.
$$\sigma_{c3} = f_c \eta_{fc} \eta_\tau$$

The effectiveness factor that accounts for the presence of the initial cracks in concrete (in-plane failure) is then estimated as

54.
$$\eta_\tau = \frac{2\tau_{cr}}{f_c \eta_{fc} \sin(2(\theta_{cr} - \theta))} - \frac{\sigma_{c1}}{f_c \eta_{fc}} \le 1$$

where τ_{cr} is the amount of shear stress that can be transferred through a crack and σ_{c1} is the average tensile stress in a concrete strut.

The average tensile stress of a strut can be estimated based on the crack spacing, which is assumed to be equal to 1·5 times the bond length (Marti *et al*., 1998), and the steel to concrete bond stress

55.
$$\sigma_{c1} = \frac{3}{16} \tau_b$$

When the contact forces develop at 45° from the crack surface, τ_{cr} can be evaluated on the basis of the proposal by Vecchio and Collins (1986) (refer to Figure 10(c))

56.
$$\tau_{cr,45°} = \frac{\sqrt{f_c}}{0·31 + [24w_{ini}/(D_{max} + 16)]}$$

where w_{ini} is the initial crack width and D_{max} is the maximum aggregate diameter (mm) ($D_{max} = 0$ for $f_c > 60$ MPa).

The minimum shear stress that can be transferred through a crack corresponds to the case in which the direction of the principal compressive stress is parallel to the face of a crack (see Figure 10(c)). Based on the work of Randl (2013) this can be estimated as

57.
$$\tau_{cr,min} = 0·2\sqrt[3]{f_c} + \begin{pmatrix} 0·8 \text{ if } f_c \le 35 \text{ MPa} \\ 1·0 \text{ if } f_c > 35 \text{ MPa} \end{pmatrix} [(f_{y,dow,x} - \sigma_{sx})\rho_x \sin\theta_{cr} + (f_{y,dow,z} - \sigma_{sz})\rho_z \cos\theta_{cr}]$$

where ρ_x is the horizontal reinforcement ratio, ρ_z is the vertical reinforcement ratio, σ_{sx} is the steel stress in the *x*-direction, $f_{y,}$ dow,x is the dowelled steel strength in the *x*-direction, σ_{sz} is the steel stress in the *z*-direction and $f_{y,dow,z}$ is the dowelled steel strength in the *z*-direction.

For other values of the angle $\theta_{cr} - \theta$, τ_{cr} can be calculated as (refer to Figure 10(c))

58.
$$\tau_{cr} = \tau_{cr,min} + \sqrt{2} \sin(\theta_{cr} - \theta)(\tau_{cr,45°} - \tau_{cr,min})$$

This assumption is based on the fact that the amount of shear that can be transferred through a crack increases quite quickly as the stress field starts to rotate (Vecchio and Collins, 1986) and then stabilises as θ_{cr} and θ become close to perpendicular. After analysis of 77 RC panels, the proposed law showed good agreement with the test results, although the authors acknowledge that future work is required to verify its general consistency.

The last remaining effectiveness factor from Equation 46 is η_{dow}, which takes into account the presence of the confining concrete struts. As previously mentioned, the enhanced concrete compressive strength along the region influenced by the dowelling was used to equilibrate the shear forces of the rebar (see Figure 6(c)). This means that this region of the concrete cannot be included in carrying any compressive stresses in the principal direction. This effect can be taken into account using

59.
$$\eta_{dow} = \frac{f_{cc}}{f_c} \ge 1·0$$

It is import to emphasise that even in the case when the yield strength of the reinforcement is not reduced due to the dowelling (point B in Figure 8), the rebars will still move towards the concrete, inducing the formation of cracks and activating the confinement effects of the concrete, meaning that Equation 59 also needs to be applied in these cases.

Strength of the undamaged struts
The compressive strength of the undamaged struts is limited by the parameter η_{UDS}, which takes into account

■ the presence of the rebars in the concrete struts, governing the spalling failures (as defined in Equation 47) and limiting the in-plane strength of the concrete (adopted from Hars (2006))

■ the presence of the dowelled reinforcement (as defined in Equation 59).

It is proposed that η_{UDS} is calculated as

$$
\begin{aligned}
\eta_{UDS} = {}& s_{dow} \min \left\{ \begin{array}{l} \eta_s \\ \dfrac{\max\left\{ \begin{array}{c} 0 \\ b_w - (4c + 2\phi_{ext}) \end{array} \right\}}{b_w} + \dfrac{\min\left\{ \begin{array}{c} b_w \\ 4c + 2\phi_{ext} \end{array} \right\}}{b_w} (1 - \eta_{dow}\delta_s) \end{array} \right. \\[2mm]
& + (1 - s_{dow}) \min \left\{ \begin{array}{l} \eta_s \\ \dfrac{\max\left\{ \begin{array}{c} 0 \\ b_w - (4c + 2\phi_{ext}) \end{array} \right\}}{b_w} + \dfrac{\min\left\{ \begin{array}{c} b_w \\ 4c + 2\phi_{ext} \end{array} \right\}}{b_w} [1 - (1 - \sin\phi_s)\delta_s] \end{array} \right.
\end{aligned}
$$

60.

in which ϕ_s is the angle of friction between the rebar surface and the surrounding concrete and s_{dow} is the relative amount of undamaged struts affected by the dowelling.

The only difference between Equations 46 and 60 is the fact that the factor η_τ is now equal to one (since there are no cracks crossing the undamaged struts) and that, unlike the damaged struts, the undamaged struts are only partly affected by the dowelling. This can be seen in Figure 9(a), where the confining concrete region (marked by dashed lines) crosses the undamaged struts only in their top-right and the bottom-left. The relative width of concrete affected by the dowelling (s_{dow}) can be expressed as a function of the total width of the undamaged struts.

Based on the geometrical consideration presented in Figure 9(d), s_{dow} can be estimated using

61. $\quad \delta_{cc} = \dfrac{\cos(\theta_{cr} - \theta)}{s_{rm}} \max \left\{ \begin{array}{l} l_{dow,x} \sin\theta \\ l_{dow,z} \cos\theta \end{array} \right.$

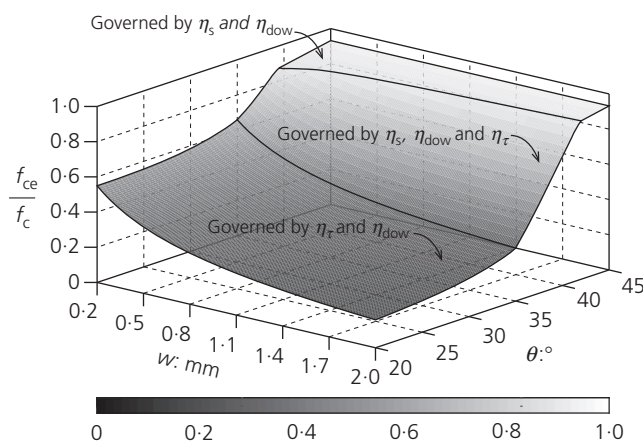62. $\quad s_{dow} = \dfrac{2\delta_{cc}}{1 - s_\tau}$

Figure 11. Representation of the failure criterion for the concrete compressive strength as a function of the stress field rotation and the crack opening at first yielding

Governing parameters

The mechanical model for the effective concrete compressive strength is quite complex and depends on a significant number of parameters (a possible strategy for solving the resulting set of equations is presented in the Appendix). However, the two parameters with the largest influence on the results are the width of the crack at the point of first yielding (w_{ini}) and the ultimate angle of the principal concrete compressive stresses. Figure 11 gives a clear view on how these two parameters influence the concrete compressive strength effectiveness factor.

As shown in Figure 11, there are three different regions in the failure surface. The first corresponds to the situation in which the rotation of the stress field is quite limited (see Figure 12(a)). For these cases, the strength of the damaged and undamaged struts is governed by the presence of the spalling cracks (η_s) and the dowelling action (η_{dow}). It can be seen that the width of the initial cracks does not influence the failure criterion. Stress field rotations, on the other hand, reduce the concrete compressive strength because the amount of undamaged struts affected by the dowel action of the reinforcement increases.

As the stress field continues to rotate, the strength of the damaged struts becomes governed by the presence of in-plane cracks (η_τ), while the strength of the undamaged struts remains dependent on the out-of-plane cracks (η_s), as shown in Figure 12(b). This corresponds to the second region of the
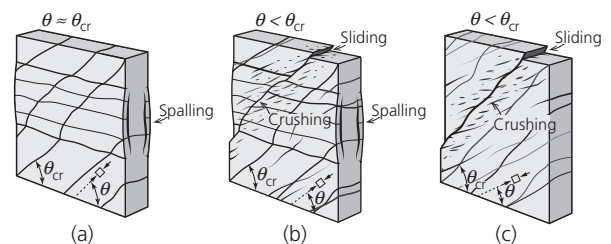

Figure 12. Potential failure mechanism of structural panels. (a) Spalling of the concrete cover in the case of small stress field rotation. (b) Spalling and combined crushing with sliding failure in the case of moderate stress field rotation. (c) Crushing and sliding of the concrete struts in the case of significant stress field rotation

Magazine of Concrete Research

Response of RC panels accounting for crack development and its interaction with rebars
Hars, Niketić and Fernández Ruiz

Table 1. Database of RC panels failing in shear

No.	Reference	Specimen ID	b_w: mm	ϕ_x: mm	ϕ_z: mm	ρ_x: %	ρ_z: %	f_c: MPa	f_{yx}: MPa	f_{yz}: MPa
1	Vecchio and Collins (1982)	PV4	70	3·43	3·43	1·06	1·06	27	242	242
2		PV6	70	6·31	6·31	1·79	1·79	30	266	266
3		PV10	70	6·31	4·72	1·79	1·00	15	276	276
4		PV11	70	6·31	5·39	1·79	1·31	16	235	235
5		PV12	70	6·31	3·15	1·79	0·45	16	469	269
6		PV16	70	4·06	4·06	0·74	0·74	22	255	255
7		PV19	70	6·31	3·99	1·79	0·71	19	458	299
8		PV20	70	6·31	4·44	1·79	0·89	20	460	297
9		PV21	70	6·31	5·37	1·79	1·30	20	458	302
10		PV22	70	6·31	5·83	1·79	1·52	20	458	420
11		PV23	70	6·31	6·31	1·79	1·79	21	518	518
12		PV25	70	6·31	6·31	1·79	1·79	19	466	466
13		PV27	70	6·31	6·31	1·79	1·79	21	442	442
14		PV28	70	6·31	6·31	1·79	1·79	19	483	483
15	Vecchio et al. (1994)	PHS2	70	8·05	5·72	3·23	0·41	66	606	521
16		PHS3	70	8·05	5·72	3·23	0·82	58	606	521
17		PHS5	70	8·05	5·72	3·23	0·41	52	606	521
18		PHS6	70	8·05	5·72	3·23	0·41	50	606	521
19		PHS8	70	8·05	5·72	3·23	1·22	56	606	521
20		PHS9	70	8·05	5·72	3·23	0·41	56	606	521
21		PHS10	70	8·05	5·72	3·23	1·22	51	606	521
22	Marti and Meyboom (1992)	PP1	287	19·54	11·28	1·94	0·65	27	479	480
23	Vecchio and Chan (1990)	PC1A	70	5·72	5·72	1·65	0·82	28	500	500
24		PC4	70	5·72	5·72	1·65	0·82	25	260	260
25	Pang and Hsu (1995)	A2	178	16·00	16·00	1·20	1·20	41	462	462
26		A3	178	19·50	19·50	1·78	1·78	42	446	446
27		A4	178	25·20	25·20	2·97	2·97	42	469	469
28		B1	178	16·00	11·30	1·20	0·60	45	462	444
29		B2	178	19·50	16·00	1·78	1·20	44	446	462
30		B3	178	19·50	11·30	1·78	0·60	45	446	444
31		B4	178	25·20	11·30	2·97	0·60	45	469	444
32		B5	178	25·20	16·00	2·97	1·20	43	469	462
33		B6	178	25·20	19·50	2·97	1·78	43	469	446
34	Zhang and Hsu (1998)	VA1	178	11·30	11·30	1·20	1·20	95	445	445
35		VA2	178	16·00	16·00	2·40	2·40	98	409	409
36		VA3	178	19·50	19·50	3·57	3·57	95	455	455
37		VA4	203	25·20	25·20	5·23	5·23	103	470	470
38		VB1	178	16·00	11·30	2·40	1·20	98	409	445
39		VB2	178	19·50	11·30	3·57	1·20	98	455	445
40		VB3	178	25·20	11·30	5·96	1·20	102	470	445
41		VB4	178	19·50	11·30	1·78	0·60	97	455	445
42	Hsu and Zhang (1997)	HB1	178	16·00	11·30	1·20	0·60	67	409	445
43		HB3	178	19·50	11·30	1·78	0·60	67	447	445
44		HB4	178	25·20	11·30	2·98	0·60	63	470	445
45	Kirschner (1986)	SE1	285	19·50	11·30	2·91	0·98	43	492	479
46		SE6	285	19·50	11·30	2·91	0·33	40	492	479
47	Watanabe and Muguruma (1989)	00R	60	6·00	6·00	0·86	0·86	28	310	310
48		15R	60	6·00	6·00	0·86	0·86	28	310	310
49		30R	60	6·00	6·00	0·86	0·86	28	310	310
50		45R	60	6·00	6·00	0·86	0·86	28	310	310
51		00D	60	7·60	7·60	0·87	0·87	28	318	318
52		30D	60	7·60	7·60	0·86	0·87	28	318	318
53		45D	60	7·60	7·60	0·87	0·87	28	318	318
54		00DI	60	7·00	7·00	1·39	1·39	31	294	294
55		22·5DI	60	7·00	7·00	1·39	1·39	31	294	294
56		45DI	60	7·60	7·60	1·30	1·30	31	318	318
57		45DII	60	7·60	7·60	2·61	2·61	31	318	318
58		45PCI	60	5·44	5·44	0·77	0·77	30	1187	1187
59		45PCII	60	5·44	5·44	1·55	1·55	30	1187	1187
60		45PCIII	60	5·44	5·44	1·55	0·77	30	1187	1187
61		45PCIV	60	5·44	5·44	1·55	0·77	45	1187	1187

Magazine of Concrete Research

Response of RC panels accounting for
crack development and its interaction
with rebars
Hars, Niketić and Fernández Ruiz

Table 1. Continued

No.	Reference	Specimen ID	b_w: mm	ϕ_x: mm	ϕ_z: mm	ρ_x: %	ρ_z: %	f_c: MPa	f_{yx}: MPa	f_{yz}: MPa
62	Kollegger and Mehlhorn (1990)	PK02	70	6·50	6·50	1·07	1·07	19	660	660
63		PK04	70	6·50	6·50	1·07	1·07	20	660	660
64		PK07	70	6·50	6·50	1·07	1·07	21	660	660
65		EGE6F1	100	6·50	6·50	0·66	0·66	16	465	465
66		EGE6F2	100	6·50	6·50	0·66	0·66	16	465	465
67		EGE6F3	100	6·50	6·50	0·66	0·66	15	465	465
68		EGE6F4	100	6·50	6·50	0·66	0·66	17	465	465
69		EGE6F7	100	6·50	6·50	0·66	0·66	19	465	465
70		EGE6F8	100	6·50	6·50	0·66	0·66	13	465	465
71		EGE7F1	100	6·50	6·50	0·66	0·66	16	660	660
72		EGE7F2	100	6·50	6·50	0·66	0·66	15	660	660
73		EGE7F3	100	6·50	6·50	0·66	0·66	17	660	660
74	Schäfer et al. (1990)	#2	100	10·00	10·00	3·14	3·14	26	582	582
75		#6	100	10·00	10·00	1·57	1·57	26	582	582
76	André (1987)	KP1	140	12·70	12·70	2·03	1·02	25	430	430
77		TP4A	70	6·35	6·35	2·03	2·03	25	450	450

failure criterion, which is dependent on the initial crack width (the wider the cracks, the larger the reduction in concrete compressive strength). The physical failure of the concrete struts in this region can occur due to spalling or crushing of the material.

As the stress field increases its rotation further, the amount of undamaged struts in the panel reduces and eventually becomes zero. This leads to the third stage of the failure criterion, when the strength of the entire panel is dependent only on the characteristics of the in-plane cracks (η_τ) (see Figure 12(c)). Once more, the influence of the initial crack width is quite pronounced and the failure mechanism of the concrete struts corresponds to crushing. Dowelling of the reinforcement affects the concrete strength of both the second and third regions of the failure surface. It has to be noted that when failure occurs by yielding of the reinforcement in both directions, the principal concrete compressive stresses do not reach $-f_{ce}$.

Experimental validation and comparison with available methods

Collected database
In order to validate the assumptions of the proposed model, a database of 77 structural panels was collected (Table 1). This database contains the results of 12 separate experimental campaigns performed by various authors. The corresponding references and the basic geometrical and mechanical properties of the panels are provided in Table 1.

The selected elements varied significantly in terms of concrete compressive strength (13–103 MPa), reinforcement ratios (0·33–5·96%) and steel yield strength (235–1187 MPa) as well as the ratio of the reinforcement placed in two perpendicular directions (from 0·11 to 1·00). The size of the specimens varied from

500 mm to 2510 mm, while their thickness varied from 60 mm to 287 mm. With respect to the loading conditions, most of the panels were subjected to pure shear (55 out of 77 specimens), some combined shear with compression (19 out of 77 specimens) and a few were loaded to shear and biaxial traction (three out of the 77 panels). The panels experienced different failure modes (concrete spalling, crushing or sliding) and while some failed due to weakening of the concrete, others failed due to yielded reinforcement in both directions.

Comparison with test database
In order to assess the accuracy of the presented approach and compare it with some of the existing strain-based approaches, the database shown in Table 1 was assessed using the elastic–plastic stress field (EPSF) method (Fernández Ruiz and Muttoni, 2007), implementing the softening equation proposed by Vecchio and Collins (1986). Table 2 summarises the results of both analyses and gives the ultimate strength assessment for each approach. It can be seen that both approaches provide satisfactory accuracy. However, the proposed mechanical procedure shows a higher level of accuracy (average of 1·01 compared with 1·11 for the EPSF approach) and lower scatter of the results (0·12 compared with 0·15 for EPSF). Additionally, it provides information on the governing failure modes, which matched those observed in the 77 test specimens.

The ratios of the measured to estimated strengths are also presented in Figure 13 as a function of four basic parameters – the concrete compressive strength f_c, the reinforcement ratio in the x-direction ρ_x, the reinforcement ratio in the z-direction ρ_z and the steel strength in the z-direction (which was the weaker direction) f_{yz}. Each of the plots shows a curve which gives the average value of the five nearest τ_{test}/τ_{model} points (with respect to a given parameter) from the entire database. As shown in the figure, the proposed mechanical approach gave consistent results over the investigated domain and showed no clear

Magazine of Concrete Research

Response of RC panels accounting for
crack development and its interaction
with rebars
Hars, Niketić and Fernández Ruiz

Table 2. Results of the EPSF analysis and the mechanical model proposed in this paper

No.	Reference	Specimen ID	τ_{test}: MPa	τ_{EPSF}: kN	τ_{model}: kN	$\tau_{test}/,\tau_{EPSF}$	τ_{test}/τ_{model}
1	Vecchio and Collins (1982)	PV4	2·84	2·56	2·62	1·11	1·08
2		PV6	4·47	4·76	4·81	0·94	0·93
3		PV10	3·97	3·69	3·73	1·08	1·06
4		PV11	3·56	3·59	3·63	0·99	0·98
5		PV12	3·13	2·55	3·05	1·23	1·03
6		PV16	2·14	1·89	1·95	1·13	1·10
7		PV19	3·96	3·73	4·01	1·06	0·99
8		PV20	4·26	4·22	4·46	1·01	0·96
9		PV21	5·03	5·18	5·46	0·97	0·92
10		PV22	6·07	6·39	7·11	0·95	0·85
11		PV23	8·88	7·69	8·09	1·15	1·10
12		PV25	9·13	8·39	7·58	1·09	1·20
13		PV27	6·35	6·74	7·94	0·94	0·80
14		PV28	5·61	5·89	6·56	0·95	0·86
15	Vecchio *et al.* (1994)	PHS2	6·66	5·18	5·21	1·29	1·28
16		PHS3	8·10	7·67	7·92	1·06	1·02
17		PHS5	4·81	3·54	3·96	1·36	1·21
18		PHS6	7·62	7·30	7·80	1·04	0·98
19		PHS8	10·84	9·53	9·91	1·14	1·09
20		PHS9	9·16	7·52	7·87	1·22	1·16
21		PHS10	8·25	7·57	7·82	1·09	1·05
22	Marti and Meyboom (1992)	PP1	4·95	5·11	4·79	0·97	1·03
23	Vecchio and Chan (1990)	PC1A	5·61	5·84	6·05	0·96	0·93
24		PC4	4·84	5·10	5·75	0·95	0·84
25	Pang and Hsu (1995)	A2	5·37	5·54	6·13	0·97	0·88
26		A3	7·65	7·94	8·49	0·96	0·90
27		A4	11·31	11·91	14·08	0·95	0·80
28		B1	3·96	3·82	4·54	1·04	0·87
29		B2	6·13	6·63	7·25	0·92	0·85
30		B3	4·35	4·59	4·89	0·95	0·89
31		B4	5·06	5·50	5·60	0·92	0·90
32		B5	7·15	8·27	8·03	0·86	0·89
33		B6	9·14	9·96	10·11	0·92	0·90
34	Zhang and Hsu (1998)	VA1	6·16	5·34	6·19	1·15	0·99
35		VA2	9·73	9·84	10·62	0·99	0·92
36		VA3	15·08	16·25	16·91	0·93	0·89
37		VA4	21·42	21·05	21·36	1·02	1·00
38		VB1	7·50	7·25	7·82	1·03	0·96
39		VB2	9·14	9·32	8·94	0·98	1·02
40		VB3	9·71	10·55	10·20	0·92	0·95
41		VB4	4·86	4·66	6·28	1·04	0·77
42	Hsu and Zhang (1997)	HB1	4·32	3·63	4·41	1·19	0·98
43		HB3	4·89	4·62	6·28	1·04	0·97
44		HB4	5·33	5·84	5·85	0·91	0·91
45	Kirschner (1986)	SE1	6·77	7·52	7·32	0·90	0·92
46		SE6	3·76	3·92	3·96	0·96	0·95
47	Watanabe and Muguruma (1989)	00R	3·14	2·66	2·72	1·18	1·15
48		15R	3·15	2·66	2·72	1·18	1·16
49		30R	3·13	2·66	2·72	1·18	1·15
50		45R	3·42	2·66	2·72	1·29	1·26
51		00D	2·97	2·70	2·83	1·10	1·05
52		30D	2·56	2·70	2·82	0·95	0·91
53		45D	2·84	2·70	2·83	1·05	1·00
54		00DI	4·96	4·10	4·17	1·21	1·19
55		22·5DI	5·06	4·10	4·17	1·23	1·21
56		45DI	3·97	4·15	4·21	0·96	0·94
57		45DII	7·61	8·29	8·35	0·92	0·91
58		45PCI	7·78	6·55	9·26	1·19	0·84
59		45PCII	11·72	8·39	11·46	1·40	1·02
60		45PCIII	9·44	7·35	9·51	1·29	0·99
61		45PCIV	10·63	8·65	11·12	1·23	0·96

Magazine of Concrete Research

Response of RC panels accounting for crack development and its interaction with rebars
Hars, Niketić and Fernández Ruiz

Table 2. Continued

No.	Reference	Specimen ID	τ_{test}: MPa	τ_{EPSF}: kN	τ_{model}: kN	$\tau_{test}/,\tau_{EPSF}$	τ_{test}/τ_{model}
62	Kollegger and Mehlhorn (1990)	PK02	9·12	7·40	8·39	1·23	1·09
63		PK04	8·91	6·64	8·75	1·34	1·02
64		PK07	9·04	6·79	9·06	1·33	1·00
65		EGE6F1	8·00	6·01	7·28	1·33	1·10
66		EGE6F2	8·10	5·68	7·37	1·43	1·10
67		EGE6F3	6·90	5·17	6·72	1·34	1·03
68		EGE6F4	7·20	5·71	7·69	1·26	0·94
69		EGE6F7	8·50	7·32	8·67	1·16	0·98
70		EGE6F8	7·35	5·23	6·03	1·40	1·22
71		EGE7F1	8·20	5·89	7·28	1·39	1·13
72		EGE7F2	7·70	5·32	7·00	1·45	1·10
73		EGE7F3	8·70	6·47	7·93	1·35	1·10
74	Schäfer et al. (1990)	#2	11·78	10·94	9·94	1·08	1·18
75		#6	14·07	9·30	10·93	1·51	1·29
76	André (1987)	KP1	5·62	6·08	5·79	0·93	0·97
77		TP4A	8·72	8·00	9·20	1·09	0·95
	Average					1·11	1·01
	Coefficient of variation					0·15	0·12

trends with respect to the four parameters, which is satisfactory. Figure 14 compares the accuracy of the presented approach with the EPSF method (Fernández Ruiz and Muttoni, 2007) implementing the softening equation proposed by Vecchio and Collins (1986) with respect to the stress field rotation. As can be seen, the mechanically-based model showed better accuracy for panels with small rotations when compared to the Vecchio and Collins (1986) approach but, most importantly, it also showed greater precision for panels with large rotations, which is relevant for the analysis of pre-stressed concrete beams. However, it should be noted that the number of panels that experienced significant stress field rotations was not large, and more specimens are required in order to consolidate these results.

Detailed analysis and comparison with other models

In order to compare the proposed mechanical procedure with existing strain-based approaches for estimating the effective concrete compressive strength, the ratio between the effective and cylinder concrete compressive strengths (f_{ce}/f_c) of each panel is shown as a function of its average principal tensile strain (ε_1) in Figure 15. The curve in the graph corresponds to the concrete compressive strength reduction factor according to Vecchio and Collins (1986). It can be seen that the results of the mechanical approach are consistent with the semi-empirical equation established within the MCFT (Vecchio and Collins, 1986). Panels with smaller average tensile strains had smaller reduction factors and vice versa. However, unlike in the MCFT equations, the mechanical efficiency factor can never be equal to one. Even in panels with relatively low-strength concrete ($f_c < 30$ MPa), the presence of reinforcement will always induce in-plane cracks and therefore reduce its effective compressive strength. This theoretical result is in

agreement the semi-empirical formulas proposed by Hsu and Zhang (1997) and Kaufmann and Marti (1998).

Conclusions

The behaviour of panels subjected to in-plane forces was investigated and a model to describe their behaviour and potential failure modes was described. The main conclusions are as follows.

- The traditional description of the phenomenon of compression softening due to transverse cracking, by means of semi-empirical equations based on transverse strains, is simple to use but does not provide information on the actual failure mode or the parameters governing failure.
- A consistent approach to this issue should account for the different stages of behaviour, namely the uncracked state, the cracked state before yielding and the cracked state after yielding with the potential development of a secondary set of cracks.
- Each stage of behaviour may be governed by different failure modes. These are out-of-plane (spalling) failures, concrete crushing and crack sliding (after rotation of the principal stress direction). These failure modes can be consistently calculated.
- Dowelling of the bars has a significant influence on the response of the member. It allows the carrying of shear through the cracks but may induce spalling of the concrete cover. In general, the various shear-carrying actions are thus not independent.
- Dowelling of the rebars does not influence the axial strength capacity of the reinforcement. However, the doweling does affect the value of concrete compressive strength.
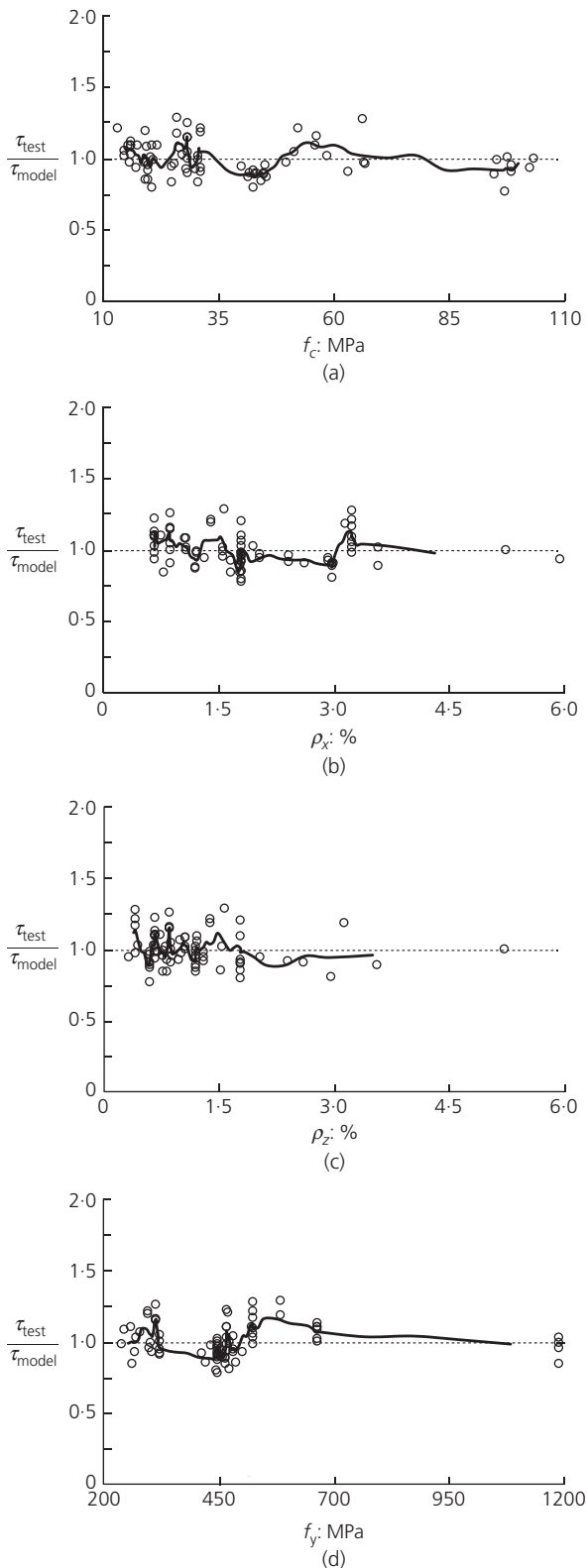
Magazine of Concrete Research

Response of RC panels accounting for crack development and its interaction with rebars
Hars, Niketić and Fernández Ruiz

Figure 13. Shear strength prediction of the database as a function of: (a) concrete compressive strength; (b) steel yield strength; (c) horizontal reinforcement ratio; (d) vertical reinforcement ratio
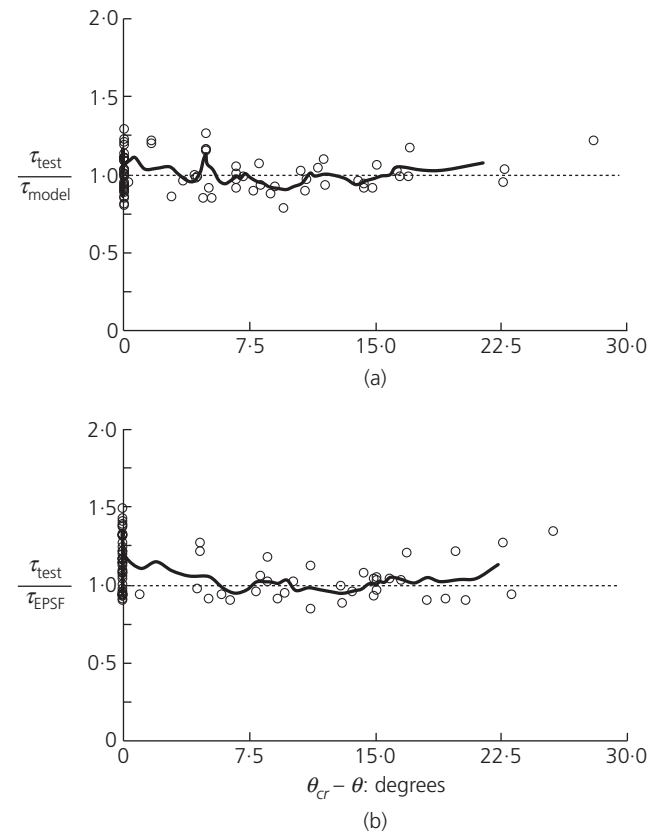

Figure 14. Shear strength prediction of the database using (a) the mechanical model presented in this paper and (b) the softening equation of Vecchio and Collins (1986) as a function of stress field rotation angle
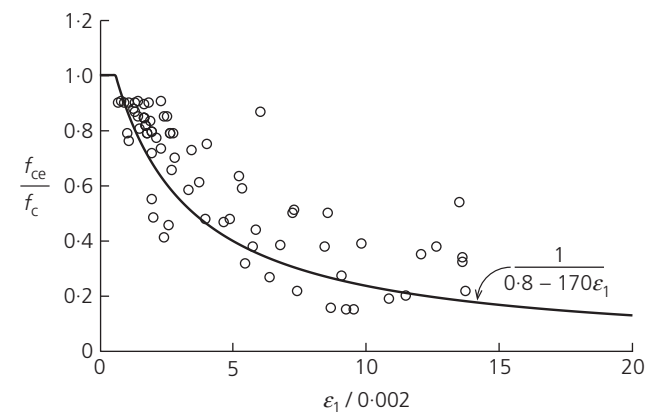
Figure 15. Calculated effective concrete compressive strength as a function of normalised principal tensile strains

■ A mechanical approach based on equilibrium and compatibility conditions can be developed, accounting for each stage of behaviour and its associated failure modes. A possible way of doing so was presented in this paper.
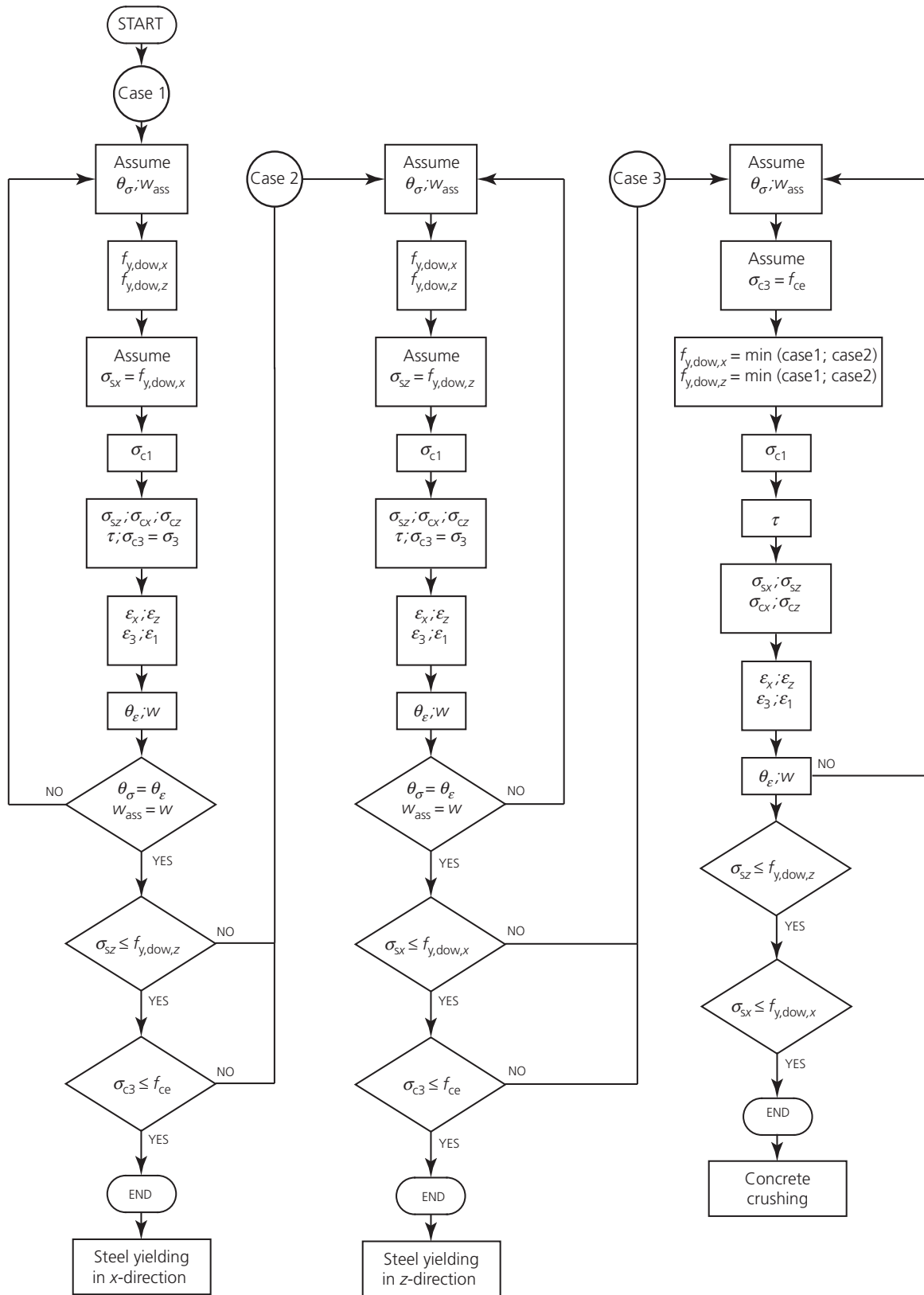
Magazine of Concrete Research

Response of RC panels accounting for crack development and its interaction with rebars
Hars, Niketić and Fernández Ruiz

Figure 16. Solving procedure at the onset of yielding

Magazine of Concrete Research

Response of RC panels accounting for crack development and its interaction with rebars
Hars, Niketić and Fernández Ruiz

■ The results of the mechanical approach show good agreement with test results (and better than those of available semi-empirical formulas) and allow for a complete description of the load–deformation response. This is important not only for accuracy, but to provide designers with a clear physical understanding of failure mechanisms and how to enhance the behaviour of a member.

Appendix: Numerical solving procedure

In order to estimate the stress and strain states of a panel, it is first necessary to define the points that correspond to the limit cases of the three stages of behaviour (the elastic uncracked phase, the onset of yielding and failure). Once these points are known, full stress–strain curves can be produced by assuming that the stress field rotates linearly in between.

Cracking of the panel

First cracking can be directly calculated on the basis of Equations 2–7.

Onset of yielding or early concrete crushing

Finding the second characterising point in a panel's load history requires the use of an iterative procedure (as presented in Figure 16). The three potential cases that can determine the behaviour of a panel are

■ case 1, which results in yielding of the reinforcement in the x-direction
■ case 2, which results in yielding of the reinforcement in the z-direction
■ case 3, which results in concrete crushing prior to yielding of the reinforcement.

After assuming the direction of the principal concrete compressive stresses (θ_σ) and the final width of the initial cracks (w_{ass}), it is possible to estimate the dowel strength of the reinforcement.

The average cracks spacing is assumed equal to be 1·5 times the bond length (Marti *et al.*, 1998), which means that the average concrete tensile stress within the cracks is equal to

63. $$\sigma_{c1} = \frac{3}{16}\tau_b$$

The principal concrete compressive stress inclination may be calculated using a Mohr circle (shown in Figure 4(b))

64. $$\tan\theta_\sigma = \frac{\tau_{xz}}{\sigma_{c1} - \sigma_{cx}}$$

Assuming that the x reinforcement yields the first $\sigma_{sx} = f_{y,dow,x}$, equilibrium conditions give

65. $$\sigma_{cx} + \rho_x f_{y,dow,x} = v_x$$

66. $$\sigma_{cz} + \rho_z \sigma_{sz} = v_z$$

67. $$\tau_{xz} = v_{xz}$$

Equations 63–67 present a system of five equations with five unknowns, which can be solved for τ_{xz}, which can then be used to determine all the required stresses in concrete and steel. The applied stress rate in each direction is usually known, meaning that v_x and v_z can be expressed using v_{xz}. The results are checked by determining the strain state of the panel and making sure that the assumed principal stress angle (θ_σ) is equal to the principal strain angle (θ_ε) and by confirming that the assumed initial crack width (w_{ass}) is equal to the calculated crack width (w).

The average strains of the panel in the x- and z-directions are equal to

68. $$\varepsilon_x = \frac{f_{yx,dow}}{E_s} - \frac{\tau_b s_{rmx}}{\phi_x E_s}$$

69. $$\varepsilon_z = \frac{\sigma_{sz}}{E_s} - \frac{\tau_b s_{rmz}}{\phi_z E_s}$$

where s_{rmx} is the average crack spacing in the x-direction (mm) and s_{rmz} is the average crack spacing in the z-direction (mm).
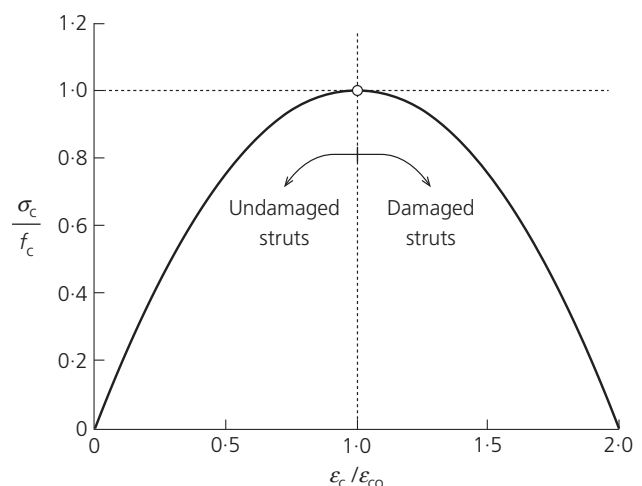

Figure 17. Stress–strain parabola for concrete compressive strength

Magazine of Concrete Research

Response of RC panels accounting for crack development and its interaction with rebars
Hars, Niketić and Fernández Ruiz

The principal concrete compressive strains can be determined by using the uniaxial stress–strain parabola (see Figure 17), assuming that the undamaged struts follow its ascending branch and that the damaged struts follow its descending branch

$$70. \qquad \varepsilon_3 = \varepsilon_{3c,DS} s_\tau + \varepsilon_{3c,UDS}(1 - s_\tau)$$

$$71. \qquad \varepsilon_{3c,DS} = \varepsilon_0 \left(1 + \sqrt{1 - \sigma_{c3}/f_c}\right)$$

$$72. \qquad \varepsilon_{3c,UDS} = \varepsilon_0 \left(1 - \sqrt{1 - \sigma_{c3}/f_c}\right)$$

$$73. \qquad \varepsilon_0 = 2f_c/E_c \approx -0{\cdot}002$$

Equations 68–70 define three points in the Mohr circle, which means that Figure 4(c) can be established and the principal compressive strain direction can be calculated

$$74. \qquad \tan\theta_\varepsilon = \frac{\varepsilon_x - \varepsilon_3}{\varepsilon_1 - \varepsilon_x}$$
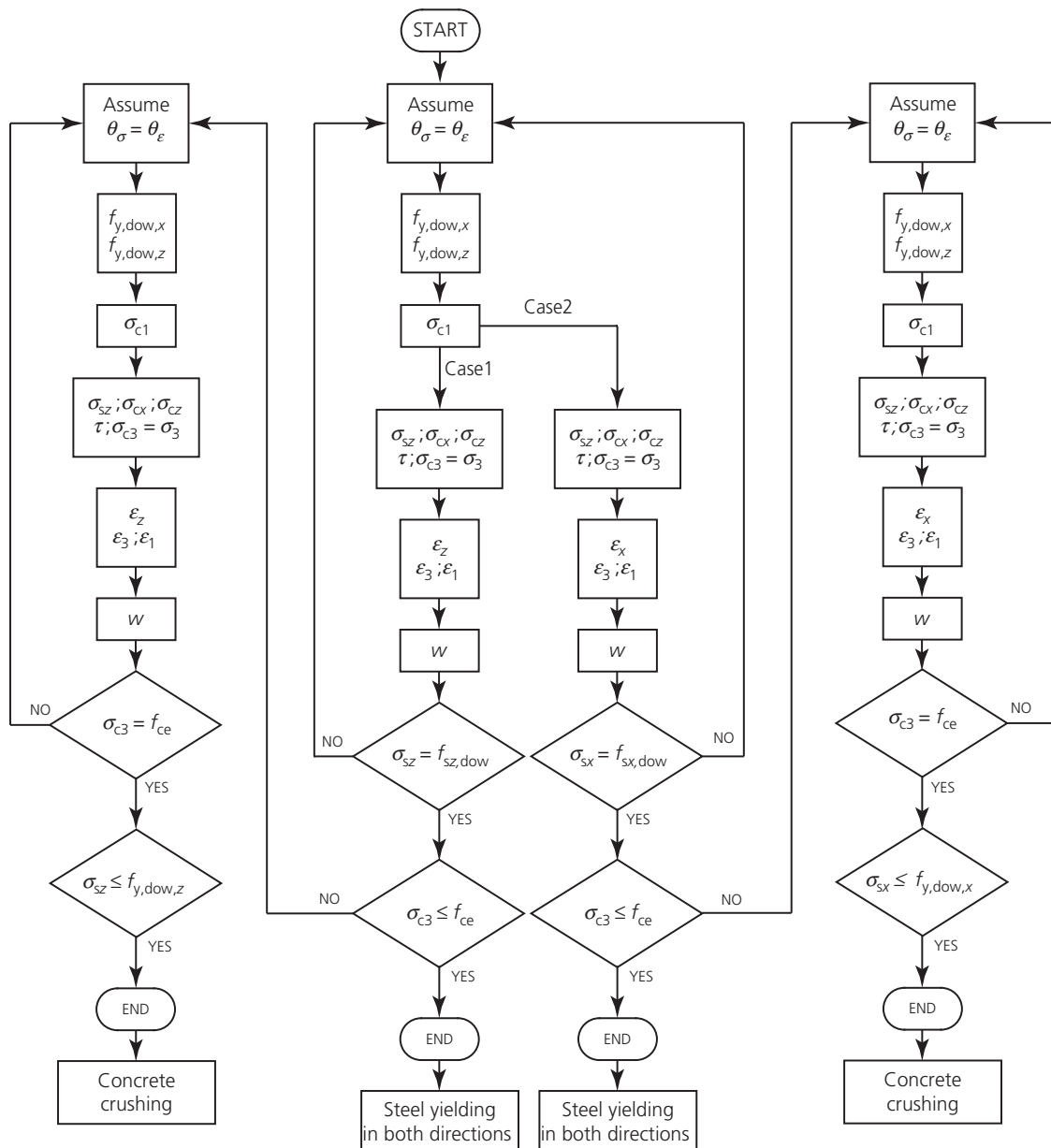

Figure 18. Solving procedure at failure

Magazine of Concrete Research

Response of RC panels accounting for crack development and its interaction with rebars
Hars, Niketić and Fernández Ruiz

Finally, it is possible to determine the initial crack opening using

$$75. \qquad w_{\mathrm{ini}} = s_{\mathrm{rm}}[\varepsilon_1 - (\sigma_{\mathrm{c1}}/E_{\mathrm{c}})]$$

As indicated in Figure 16, it is now necessary to verify that the assumed stress state is respected, or try another case if the answer does not comply with this condition.

Case 2 is almost identical to case 1, while case 3 is a bit simpler. The only difference between the solving procedure for case 1 and case 2 is in the fact that the vertical instead of the horizontal reinforcement is assumed to have reached yielding by the end of the second phase of the panel's load history. Apart from this, all the necessary validations and solving procedure are identical (see Figure 16).

The dowelled steel strength of the x-reinforcement according to case 1 is lower than that of case 3, since the angle θ is higher for case 1 than for case 3. Thus, the governing condition is crushing of the concrete struts instead of reinforcement yielding. In the same way, the dowelled steel strength of z-reinforcement according to case 2 is lower than that of case 3. These two values for both dowelled steel strengths (of cases 1 and 2) are adopted for case 3, which is a slightly conservative simplification.

Failure of the panel

In order to determine the third (and final) characteristic point of the panel's load history, another iterative procedure needs to be applied. Looking at the scheme shown in Figure 18, it can be seen that, depending on the determining case from Figure 16, it is now possible to estimate the average strain in one direction (ε_x in case 2 or ε_z in case 1).

The direction of the principal compressive stresses is assumed to be parallel to the direction of the principal compressive strains. The secondary dowelling should only be applied on the reinforcement that did not yield during the previous phase (x-direction in case 2 and z-direction in case 1). The additional dowelling should only be applied on the remaining steel stresses in the reinforcement that yields second, from the onset of the yielding of the direction of the first yielded reinforcement.

The stress field rotates until failure of the concrete or steel. The stress and strain transformations that were applied at the onset of yielding should be applied during this phase as well. At the end of the solving procedure, it is verified that the ultimate stress direction is lower than that at the onset of yielding.

REFERENCES

ACI (American Concrete Institute) (2008) ACI 318-08: Building code requirements for structural concrete and commentary. ACI, Farmington Hills, MI, USA.

André HMO (1987) *Toronto/Kajima Study on Scale Effects in Reinforced Concrete Elements*. PhD dissertation, University of Toronto, Toronto, ON, Canada.

Belarbi A and Hsu CTT (1995) Constitutive laws of softened concrete in biaxial tension-compression. *ACI Structural Journal* **92(5)**: 562–573.

CEN (European Committee for Standardization) (2004) Eurocode 2: Design of concrete structures – part 1-1: general rules and rules for buildings. CEN, Brussels, Belgium.

Fernández Ruiz M and Muttoni A (2007) On development of suitable stress fields for structural concrete. *ACI Structural Journal* **104(4)**: 495–502.

fib (International Federation for Structural Concrete) (2011) *fib Model Code 2010, Final Draft. fib*, Lausanne, Switzerland.

Hars E (2006) *Zum Querkraftwiderstand von Stahl- und Spannbetonträgern mit dünnen Stegen*. PhD dissertation, École Polytechnique Fédérale de Lausanne, IBETON, Lausanne, Switzerland (in German).

Hsu CTT and Zhang LX (1997) Nonlinear analysis of membrane elements by fixed-angle softened-truss model. *ACI Structural Journal* **94(5)**: 483–491.

Kaufmann W and Marti P (1998) Structural concrete: cracked membrane model. *Journal of Structural Engineering* **124(12)**: 1467–1475.

Kirschner U (1986) *Investigating the Behaviour of Reinforced Concrete Shell Elements*. PhD dissertation, University of Toronto, Toronto, ON, Canada.

Kollegger J and Mehlhorn G (1990) *Experimentelle Untersuchungen zur Bestimmung der Druckfestigkeit des gerissenen Stahlbetons bei einer Querzugbeanspruchung*. Deutscher Ausschuss für Stahlbeton, Berlin, Germany, Test report no. 413 (in German).

Marti P and Meyboom J (1992) Response of prestressed concrete elements to in-plane shear forces. *ACI Structural Journal* **89(5)**: 503–514.

Marti P, Alvarez M, Kaufmann W and Sigrist V (1998) Tension chord model for structural concrete. *Structural Engineering International* **8(4)**: 287–298.

Muttoni A (1989) *Die Anwendbarkeit der Plastizitätstheorie in der Bemessung von Stahlbeton*. PhD dissertation, ETHZ, Institut für Baustatik und Konstruktion, Zürich, Switzerland (in German).

Muttoni A, Burdet O and Hars E (2006) Effect of duct type on the shear strength of thin webs. *ACI Structural Journal* **103(5)**: 729–735.

Muttoni A, Fernández Ruiz M and Niketic F (2015) Design versus assessment of concrete structures using stress fields and strut-and-tie models. *ACI Structural Journal* **112(5)**: 605–616.

Nielsen MP and Hoang LC (2011) *Limit Analysis and Concrete Plasticity*, 3rd edn. CRC Press, Boca Raton, FL, USA.

Okamura H and Maekawa K (1991) *Nonlinear Analysis and Constitutive Methods of Reinforced Concrete*. University of Tokyo, Tokyo, Japan.

Pang XBD and Hsu CTT (1995) Behavior of reinforced concrete membrane elements in shear. *ACI Structural Journal* **92(6)**: 665–667.

Randl N (2013) Design recommendations for interface shear transfer in *fib* model code 2010. *Structural Concrete* **14(3)**: 230–241.

Rasmussen BH (1962) Strength of transversely loaded bolts and dowels cast into concrete. *Proceedings of the Danish Society for Structural Science and Engineering* **34(2)**: 39–55.

Schäfer K, Schelling G and Kuchler T (1990) *Druck und Querzug in Bewehrten Betonelementen*. Deutscher Ausschuss für Stahlbeton, Berlin, Germany, Test report no. 408 (in German).

Sorensen JH, Hoang LH, Olesen JF and Fischer G (2016) Catenary action in rebars crossing a casting joint loaded in shear. In *Proceedings of the 11th fib International PhD Symposium in Civil Engineering, Tokyo, Japan* (Maekawa K, Kasuga A and Yamazaki J (eds)). University of Tokyo, Tokyo, Japan, pp. 735–742.

Magazine of Concrete Research

Response of RC panels accounting for crack development and its interaction with rebars
Hars, Niketić and Fernández Ruiz

Tepfers R (1979) Cracking of concrete cover along anchored deformed reinforcing bars. *Magazine of Concrete Research* **31(106)**: 3–12, http://dx.doi.org/10.1680/macr.1979.31.106.3.

Vecchio FJ (2000) Disturbed stress field model for reinforced concrete: formulation. *Journal of the Structural Division ASCE* **126(9)**: 1070–1077.

Vecchio FJ and Chan CCL (1990) Reinforced concrete membrane elements with perforations. *ASCE Journal of Structural Engineering* **116(9)**: 2344–2360.

Vecchio FJ and Collins MP (1982) *Response of Reinforced Concrete to In-Plane Shear and Normal Stresses*. Department of Civil Engineering, University of Toronto, Toronto, ON, Canada.

Vecchio FJ and Collins MP (1986) The modified compression-field theory for reinforced concrete elements subjected to shear. *ACI Structural Journal* **83(2)**: 219–231.

Vecchio FJ, Collins MP and Aspiotis J (1994) High-strength concrete elements subjected to shear. *ACI Structural Journal* **91(4)**: 423–433.

Vintzeleou E and Tassios TP (1990) Eccentric dowels loaded against core of concrete sections. *Journal of Structural Engineering* **116(10)**: 2621–2633.

Watanabe F and Muguruma H (1989) Ultimate strength and deformations of RC panel. *ASCE Structural Congress: Proceedings of Sessions Related to Structural Design Analysis and Testing, San Francisco, CA, USA*. American Society of Civil Engineers, New York, NY, USA, pp. 31–38.

Zhang IX and Hsu TTC (1998) Behavior and analysis of 100 MPa concrete membrane elements. *Journal of Structural Engineering* **124(1)**: 24–34.

How can you contribute?

To discuss this paper, please submit up to 500 words to the editor at journals@ice.org.uk. Your contribution will be forwarded to the author(s) for a reply and, if considered appropriate by the editorial board, it will be published as a discussion in a future issue of the journal.